THE JOURNAL OF PHYSICAL CHEMISTRY C

Article

pubs.acs.org/JPCC

Epitaxial Growth of Cu_2O on Ag Allows for Fine Control Over Particle Geometries and Optical Properties of Ag−Cu_2O Core−Shell Nanoparticles

Hao Jing,[†,§] Nicolas Large,[‡,⊥] Qingfeng Zhang,[†] and Hui Wang*[,†]

[†]Department of Chemistry and Biochemistry, University of South Carolina, 631 Sumter Street, Columbia, South Carolina 29208, United States

[‡]Department of Physics and Astronomy, Department of Electrical and Computer Engineering, Laboratory for Nanophotonics, Rice University, Houston, Texas 77005, United States

Supporting Information

ABSTRACT: We demonstrate that Ag−Cu_2O core−shell nanoparticles exhibit geometry-dependent optical properties that are highly tunable across the visible and near-infrared spectral regions. We have developed a robust wet chemistry approach to the geometry control of Ag−Cu_2O core−shell nanoparticles through epitaxial growth of Cu_2O nanoshells on the surfaces of various Ag nanostructures, such as quasi-spherical nanoparticles, nanocubes, and nanocuboids. Precise control over the core and the shell geometries enables us to develop detailed, quantitative understanding of how the Cu_2O nanoshells introduce interesting modifications to the resonance frequencies and the extinction spectral line shapes of multiple plasmon modes of the Ag cores. Finite-difference time-domain calculations provide further insights into the physical origin and the geometry-dependence of the various plasmon modes observed in the Ag−Cu_2O core−shell nanoparticles.

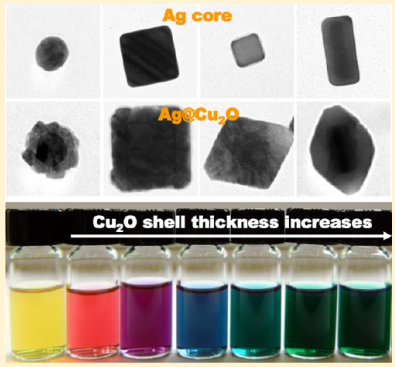

INTRODUCTION

Heterostructured core−shell nanoparticles exhibit a series of intriguing optical, electronic, and catalytic properties that arise from the nanoscale interactions between the core and the shell.[1−7] Recent advances in the geometry-controlled synthesis of colloidal core−shell nanoparticles allow for the fine-tuning of the synergistic properties of the particles through deliberate control over important geometric parameters, such as the core shape, the shell architectures, the compositional arrangement, and the interfacial structures. As well-demonstrated in several binary heteronanostructures, such as CdSe-CdS,[8−11] Au−Ag,[12−19] Pd−Pt,[20−23] and Au−Pd,[13,19,24−30] the formation of monocrystalline, conformal core−shell structures involves the epitaxial growth of the shell on the core, which typically requires small lattice mismatches (<∼ 5%) between the core and the shell materials. By judiciously tailoring the core−shell interfaces and the shell growth kinetics, the formation of bimetallic core−shell nanostructures through epitaxial growth has recently become possible even between materials with relatively large lattice mismatches, such as Pd−Cu (7.1% lattice mismatch),[31,32] Au−Cu (11.4% lattice mismatch),[33] and Au−Ni (13.6% lattice mismatch).[34] For metal−semiconductor hybrid nanostructures, however, the formation of epitaxial core−shell nanoparticles remains significantly more challenging primarily due to the structural dissimilarity and relatively large lattice mismatches between the metal and the semiconductor components.[35] Although synthetically challenging, a variety of metal−semiconductor core−shell nanostructures have been fabricated through nonepitaxial shell growth approaches.[35−43] The capabilities to tailor the particle geometries enable the observation of a series of interesting optical phenomena, such as enhanced optical absorption,[42] reinforced plasmonic tunablitiy,[38,43] exciton−plasmon coupling,[6,41,44] and the occurrence of Fano resonances,[45] in various metal−semiconductor core−shell nanoparticle systems.

Hybrid nanoparticles composed of a noble metal core and a Cu_2O shell represent an interesting metal−semiconductor heteronanostructure with geometrically tunable optical properties.[38,46−56] On one hand, coating the surfaces of a metallic nanoparticle with a Cu_2O nanoshell gives rise to drastically enhanced plasmonic tunability.[38,50,51] It has been demonstrated that the localized plasmon resonance frequencies of Au−Cu_2O core−shell nanoparticles are sensitively dependent on the size of the core, the thickness of the shell, the porosity of the shell, and the spacing between the core and the shell.[38,50,51] The real part of the dielectric permittivity of Cu_2O is responsible for the shift of the plasmon resonances, whereas its imaginary part further modulates the extent of plasmon damping and the relative contributions of absorption and scattering to the overall optical extinction.[50] On the other hand, the presence of the metallic core also significantly enhances the photocatalytic performance of the semiconducting Cu_2O shell.[52−55] The

Received: June 27, 2014
Revised: July 31, 2014
Published: August 7, 2014

enhanced photocatalysis observed on Au−Cu_2O and Ag−Cu_2O core−shell nanoparticles have been interpreted as a consequence of the enhancement of electron−hole pair generation in the Cu_2O shell through direct electron transfer (DET) and plasmon-induced resonant energy transfer (PIRET).[52,53]

Developing detailed, quantitative understanding of the structure−property relationship requires fine control over both the core and the shell geometries. Much success has recently been achieved on the geometry-controlled synthesis of Au−Cu_2O core−shell nanoparticles through either epitaxial or nonepitaxial shell growth processes.[38,46−51,55,56] It has been reported that submicron-thick Cu_2O shells can be grown on Au nanoparticles through a hollow shell-refilling (HSR) process.[47,49] The resulting Au−Cu_2O core−shell particles well-preserved the morphologies of the Au cores and exhibited optical extinction features dominated by the Mie scattering from the thick Cu_2O shells.[47,49] We recently demonstrated that Cu_2O nanocrystallites could be hierarchically assembled on the surface of Au cores to form Au−Cu_2O core−shell nanoparticles with porous polycrystalline Cu_2O shells.[38,50] Through Ostwald ripening of the polycrystalline Cu_2O shells, spacing between the Au core and the Cu_2O shell can be controllably created, giving rise to the formation of an interesting yolk−shell structure.[38] Epitaxial growth of Cu_2O nanoshells on the surfaces of quasi-spherical Au nanoparticles led to the formation of Au−Cu_2O core−shell nanoparticles with dense Cu_2O shells.[50,51] By controlling the size of the Au cores and the thickness of the epitaxial Cu_2O shells, the plasmon resonances of the core−shell particles can be fine-tuned over a broad spectral range across the visible and near-infrared regions.[50,51] More recently, Cu_2O nanoshells have been grown on Au nanorods and Au nanopolyhedra, resulting in the formation of geometrically more complicated Au−Cu_2O core−shell heteronanostructures enclosed by multiple well-defined facets.[46−48,55]

In this paper, we focus on the controlled synthesis and tunable optical properties of Ag−Cu_2O core−shell nanoparticles of various geometries. We report a general method for the geometry control of Ag−Cu_2O core−shell nanoparticles through epitaxial growth of Cu_2O nanoshells on the surfaces of various Ag nanostructures, such as quasi-spherical nanoparticles, nanocubes, and nanocuboids. In comparison to other noble metal counterparts, such as Au, Pd, Pt, and Cu, Ag nanoparticles have far stronger plasmon resonances, wider optical tuning range, more intense near-field enhancements, and greater refractometric plasmon sensitivity.[57] Because of significantly less plasmon damping in Ag, a series of higher-order multipolar plasmon resonances become experimentally observable in the optical extinction spectra of Ag nanospheres,[58] nanocubes,[59−61] nanopolyhedra,[62] and nanorice[63] when the particle dimensions reach the subwavelength size regime, whereas the extinction spectral features of Au nanoparticles of the same shapes and dimensions are more dominated by the dipole plasmon resonances. As demonstrated in this work, tight geometry control of Ag−Cu_2O core−shell nanoparticles through the expitaxial growth of a continuous Cu_2O nanoshell on Ag cores allows one to study, in great detail, how the Cu_2O shell introduces interesting modifications to the resonance frequencies and the extinction spectral line shapes of various plasmon modes of the Ag core. The understanding of the geometry-property relationship of the Ag−Cu_2O core−shell nanoparticles has been further enhanced by finite-difference time-domain (FDTD) calculations.

EXPERIMENTAL SECTION

Materials. All chemicals were obtained from commercial suppliers and used without further purification. Hexadecyltrimethylammonium bromide (CTAB, >98%) and 5-bromosalicylic acid (>98%) were purchased from TCI America. Ethylene glycol (EG) was purchased from J. T. Baker. Sodium hydroxide (NaOH) and sodium chloride (NaCl) were purchased from Fisher Scientific. Polyvinylpyrrolidone (PVP, average MW 58 000), hydrogen tetrachloroaurate trihydrate ($HAuCl_4·3H_2O$, ACS, 99.99% metals basis), silver nitrate ($AgNO_3$, 99.9995% metals basis), hydrazine ($N_2H_4·3H_2O$, 35 wt % solution in water), and hexadecyltrimethylammonium chloride (CTAC, 96% powder) were purchased from Alfa Aesar. L-Ascorbic acid (BioUltra, ≥99.5%), sodium borohydride ($NaBH_4$, 99%), hydrochloric acid (HCl, 37 wt % in water), silver trifluoroacetate (CF_3COOAg, ≥99.99% trace metals basis), and sodium hydrosulfide hydrate ($NaHS·xH_2O$) were purchased from Sigma-Aldrich. Ultrapure water (18.2 MΩ resistivity, Barnstead EasyPure II 7138) was used for all experiments. All glassware was cleaned using freshly prepared aqua regia (HCl/HNO_3 in a 3:1 ratio by volume) followed by thorough rinse with copious amount of water.

Synthesis of Ag Quasi-Spherical Nanoparticles. AgCl colloids were first synthesized and then used as the precursor for the fabrication of monodisperse Ag quasi-spherical nanoparticles following a previously published protocol[64] with some minor modifications. In a typical procedure, 0.425 g PVP was dissolved in 100 mL of water under magnetic stir followed by the introduction of 0.425 g $AgNO_3$. Then 1.0 mL of 5 M NaCl was added, and the mixture was stirred for another 15 min in the dark to form colloidal suspensions of AgCl. To synthesize quasi-spherical Ag nanoparticles around 40 nm in diameter, 100 mL of 50 mM ascorbic acid, 13 mL of 0.5 M NaOH, and 12.5 mL of freshly prepared AgCl colloids were mixed under magnetic stir. The mixture was then stirred at room temperature for 2 h in the dark. The products were centrifuged (6000 rpm, 7 min), washed with water twice, and finally redispersed in 14 mL of water and stored in a refrigerator at 4 °C for future use. The particle concentration was ∼1.0×10^{12} particles mL^{-1}. The protocol for the preparation of ∼100 nm Ag nanoparticles was the same except that 11 mL of 0.5 M NaOH was added. The particle concentration of the as-obtained 100 nm Ag colloids was ∼1.5×10^{11} particles mL^{-1}.

Synthesis of ∼40 nm Ag Nanocubes. The ∼40 nm Ag nanocubes with truncated corners were prepared following the protocol developed by Xia and co-workers[65] with slight modifications. Briefly, 40 mL of ethylene glycol (EG) was added into a 100 mL round-bottom flask and preheated under magnetic stir in an oil bath set to 150 °C for about 40 min. Then 500 μL of 3 mM NaHS solution, 3 mL of 3 mM HCl, and 10 mL of PVP (100 mg/mL) were added sequentially. After stirring the mixture for 2 min, 3 mL of 282 mM CF_3COOAg solution was added. During the entire process, the flask was capped with a glass stopper except during the addition of reagents. After 22 min, the reaction was quenched in an ice−water bath when the suspension had reached a brown color with a characteristic plasmon resonance peak at ∼420 nm in the extinction spectrum. The Ag nanocubes were centrifuged (8000 rpm, 8 min), washed with acetone and then water, and finally redispersed in 6 mL of EG. The particle concentration of the 40 nm nanocubes was 3.0×10^{12} particles mL^{-1}.

dx.doi.org/10.1021/jp5064116 | J. Phys. Chem. C 2014, 118, 19948−19963

Synthesis of ~100 nm Ag Nanocubes. Larger Ag nanocubes with average edge length of ~100 nm were prepared through a seed-mediated growth process.[65] Typically, 10 mL of EG was added into a 50 mL round-bottom flask and heated in an oil bath at 150 °C under magnetic stir. After 10 min, 3 mL of PVP (250 mg/mL in EG) was added. After another 10 min, 200 μL of colloidal suspension of ~40 nm Ag nanocubes was introduced, followed by the addition of 2 mL of 282 mM $AgNO_3$. After 20 min, the reaction was quenched by immersing the reaction mixture in an ice−water bath. The product was centrifuged (8000 rpm, 8 min), washed with acetone and then water, and finally redispersed in 5 mL of EG for future use. The particle concentration of the 100 nm nanocubes was 1.0×10^{11} particles mL^{-1}.

Synthesis of Au−Ag Core−Shell Nanocuboids. Au nanorods were fabricated using a recently published seed-mediated growth method[66] and used as the core for the subsequent growth of Au−Ag core−shell nanocuboids. To prepare the seed solution, 5 mL of 0.5 mM $HAuCl_4$ was first mixed with 5 mL of 0.2 M CTAB solution in a 20 mL scintillation vial. Then 1 mL of freshly prepared 6 mM $NaBH_4$ was quickly injected into the Au(III)-CTAB solution under vigorous magnetic stir (1200 rpm). The solution color changed from yellow to brownish-yellow, and the stir was stopped after 2 min. The seed solution was aged at room temperature for 30 min before use. To prepare the growth solution, 9.0 g of CTAB and 1.1 g of 5-bromosalicylic acid were dissolved in 250 mL of water at 60 °C in a 500 mL Erlenmeyer flask. The solution was cooled to 30 °C after 48 mL of 4 mM $AgNO_3$ was added. The mixture was kept undisturbed at 30 °C for 15 min, after which 250 mL of 1 mM $HAuCl_4$ solution and 2.1 mL HCl (37 wt % in water, 12.1 M) were added. After another 15 min of magnetic stir, 1.25 mL of 0.064 M ascorbic acid was added, and the solution was vigorously stirred for 30 s until it became colorless. Finally, 0.4 mL of the seed solution was injected into the growth solution. The reactant mixture was stirred vigorously for another 30 s and left undisturbed at 30 °C for 12 h for the Au nanorod growth. The products were isolated by centrifugation at 7000 rpm for 20 min followed by removal of the supernatant. Then the nanorods were washed with water and 0.1 M CTAC and finally redispersed in 10 mL of 0.1 M CTAC. No size or shape-selective fractionation was performed.

Au−Ag core−shell nanocuboids were prepared through controlled epitaxial overgrowth of Ag on single-crystalline Au nanorods following a previous reported protocol[67] with some minor modifications. Briefly, 0.1 mL of the colloidal Au nanorods (dispersed in 0.1 M CTAC) was diluted to 1 mL with water. Various volumes (10−200 μL) of 10 mM $AgNO_3$ solution were subsequently added, followed by the addition of 50 mM ascorbic acid solutions. The volume of the ascorbic acid solution was the same as that of $AgNO_3$ solution for each aliquot. The mixtures were kept in a water bath at 65 °C for 4.5 h to ensure the complete Au shell growth. The Au−Ag core−shell nanocuboids were centrifuged (5000 rpm, 5 min), washed with water and 0.1 M CTAC once, and finally redispersed in 0.3 mL of 0.1 M CTAC solution (final concentration of 1.0×10^{11} particles mL^{-1}).

Synthesis of Ag−Cu_2O Core−Shell Nanoparticles. Ag−Cu_2O core−shell nanoparticles of various geometries were synthesized through expitaxial growth of Cu_2O nanoshells on Ag surfaces at room temperature. Typically, 80 μL of colloidal Ag quasi-spherical nanoparticles, nanocubes, or nanocuboids was first introduced into 5 mL of 2 wt % PVP aqueous solution. Various amounts (2.5−100 μL) of 0.1 M $Cu(NO_3)_2$ solution, depending on the desired thickness of the resulting Cu_2O shells, was subsequently added. Then 11.2 μL of 5 M NaOH and 5 μL of N_2H_4 solution (35 wt %, Sigma-Aldrich) were added under magnetic stir. The solutions were kept stirring for 10 min and the resulting core−shell nanoparticles were subsequently separated from the reaction mixtures by centrifugation. All Ag−Cu_2O core−shell nanoparticles were washed with water and anhydrous ethanol, and finally redispersed in ethanol for storage.

Characterizations. Transmission electron microscopy (TEM) images were obtained using a Hitachi H-8000 transmission electron microscope operated at an accelerating voltage of 200 kV. All samples for TEM measurements were dispersed in ethanol and drop-dried on 200 mesh Formvar/carbon coated Cu grids. Scanning electron microscopy (SEM) images and energy dispersive spectroscopy (EDS) results were also obtained using a Zeiss Ultraplus thermal field emission scanning electron microscope. The samples for SEM and EDS measurements were dispersed in ethanol and drop-dried on silicon wafers. The atomic-level structures of the nanoparticles were resolved by high-resolution transmission electron microscopy (HRTEM) using a JEOL 2100F 200 kV FEG-STEM/TEM microscope. The samples for HRTEM measurements were dispersed in water and drop-dried on 400 mesh Cu grids with ultrathin carbon support film (Electron Microscopy Science Inc.). The optical extinction spectra of the nanoparticles were measured on aqueous colloidal suspensions at room temperature using a Beckman coulter Du 640 spectrophotometer.

Finite-Difference Time-Domain (FDTD) Calculations. FDTD calculations were performed using a commercial FDTD software package (Lumerical Solutions). We used FDTD to calculate the optical extinction spectra of the core−shell nanoobjects and investigate the nature of the localized plasmon resonance modes in each nanostructure. Geometrical parameters were extracted from the TEM and SEM images of the nanospheres, nanocubes, and nanocuboids. Ag spherical cores had a diameter of 40 and 100 nm, Ag nanocubes had edge lengths of 40 and 100 nm, and the nanocuboid was modeled as a cylindrical Au nanorod of 90 nm in length and 18 nm in diameter with hemispherical ends surrounded by a Ag cuboidal shell. The overall (Au core)−(Ag shell) nanocuboid size was 110 nm × 50 nm. All of the three nanostructures were then coated with a Cu_2O shell with thickness of 0 to ~50 nm. Calculations were done for isolated core−shell nano-objects in water and excited by linearly polarized light. The bulk dielectric functions tabulated by Palik[68] were used for Au, Ag, and water, and the dielectric function from the Landolt−Börnstein database was used for Cu_2O.[69] Fine FDTD meshes of 1−2.5 nm were necessary to correctly describe the Cu_2O shells.

To take into account the effect of the ensemble of randomly dispersed core−shell nano-objects (nanocubes and nanobars), calculations were performed by averaging over six angular orientations with respect to the incident polarization. Moreover, as the nanocuboid was elongated, the dipolar plasmon resonances split into a longitudinal and a transverse mode, respectively. FDTD calculations of the nanocuboid were performed for both longitudinal and transverse excitations and then averaged. Surface charge distributions were calculated at the silver surface of the core−shell nano-objects for each plasmon mode and at a given orientation. The near-field enhancements were calculated both at 1.5 nm away from the

dx.doi.org/10.1021/jp5064116 | J. Phys. Chem. C 2014, 118, 19948−19963

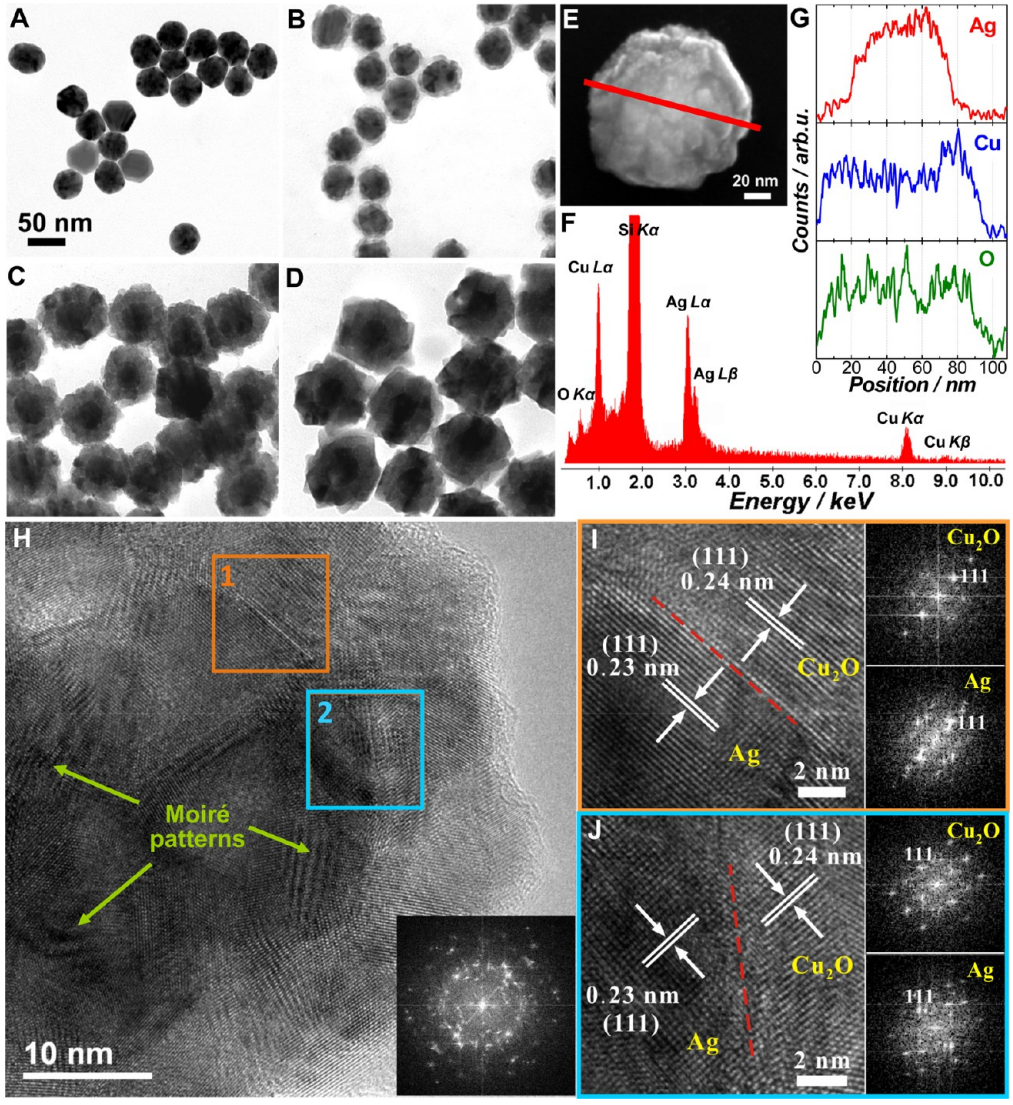

Figure 1. Growth of Cu_2O nanoshells on Ag quasi-spherical cores. TEM images of (A) Ag quasi-spherical nanoparticles (~40 nm in diameter) and Ag−Cu_2O core−shell nanoparticles with various shell thicknesses obtained by adding (B) 5 μL, (C) 40 μL, and (D) 80 μL of 100 mM $Cu(NO_3)_2$ solution. All the TEM images share the same scale bar in panel A. (E) SEM image and (F) EDS spectrum of an individual Ag−Cu_2O core−shell nanoparticle from the sample shown in panel C. (G) Spatial elemental distribution obtained from the EDS line scan measurements along the red line shown in panel E based on the L-lines of Ag and K-lines of Cu and O. (H) HRTEM image of an individual Ag−Cu_2O core−shell nanoparticle. The bottom-right inset is the fast Fourier transform (FFT) pattern of the region encompassing the whole cross section of the core−shell particle. HRTEM images showing the Au−Cu_2O interfacial structures and the corresponding FFT patterns of (I) region 1 and (J) region 2 in panel H, respectively. The red dash lines highlight the boundary between the Ag and Cu_2O. The upper right panels show the FFT patterns of the Cu_2O shell regions and the lower right panels show the FFT patterns of the Ag core regions.

Ag surface and at 1.5 nm away from the surface of the Cu_2O shells.

RESULTS AND DISCUSSION

Ag−Cu_2O Core−Shell Nanospheres. We started with a relatively simple core geometry, Ag nanospheres, on which Cu_2O layers could be epitaxially deposited to form Ag−Cu_2O core−shell nanoparticles. In comparison to spherical Au nanoparticles, the size-controlled synthesis of monodisperse spherical Ag nanoparticles has been much more challenging.[64,70,71] Here we adopted a recently developed AgCl-templated method[64] to achieve the precise control over the sizes of Ag quasi-spherical nanoparticles. As shown in Figure 1A, the as-fabricated Ag nanoparticles were highly monodisperse with uniform quasi-spherical morphology and their diameters were determined to be 40 ± 3.1 nm. By adjusting the amount of NaOH added into the reaction mixtures, the average size of Ag quasi-spherical nanoparticles could be fine-controlled in the range from ~20 nm to ~100 nm. Figure S1 in Supporting Information shows a TEM image of the larger Ag particles (100 ± 4.4 nm in diameters) fabricated using this method, which also displayed quasi-spherical morphology and high monodispersity. Both Ag and Cu_2O have the face-centered cubic (fcc) crystalline structure with lattice mismatch of ~4.2%, which makes it possible to epitaxially deposit Cu_2O on Ag surfaces under appropriate conditions. The epitaxial growth of Cu_2O shells over the surfaces of the Ag nanoparticles was conducted through the controlled reduction of $Cu(NO_3)_2$ at room temperature using hydrazine as a mild reducing agent in an aqueous solution at pH value of 11. We have previously

dx.doi.org/10.1021/jp5064116 | J. Phys. Chem. C 2014, 118, 19948−19963

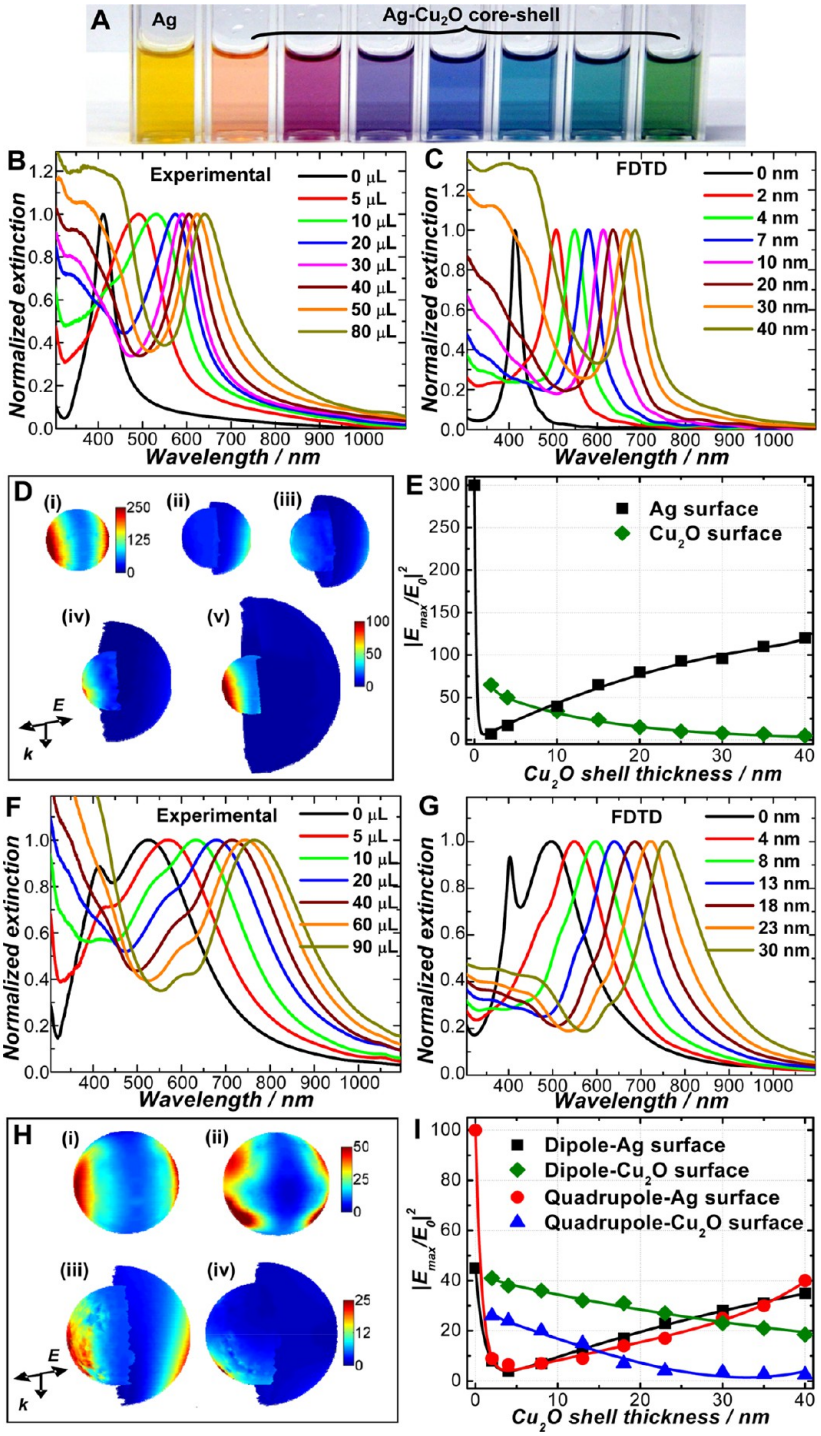

Figure 2. Tunable optical properties of Ag−Cu_2O core−shell nanospheres. (A) True color picture of colloidal Ag quasi-spherical nanoparticles (40 nm in diameter) and Ag−Cu_2O core−shell nanoparticles. From left to right, the Cu_2O shell thickness increases. The extinction spectra of these colloidal samples are shown in panel B. (B) Experimental extinction spectra of Ag nanoparticles (40 nm average diameter) and Ag−Cu_2O core−shell nanoparticles with various shell thicknesses obtained upon the addition of different volumes of 100 mM $Cu(NO_3)_2$ as indicated in the figure. (C) Calculated extinction spectra of Ag−Cu_2O core−shell nanospheres (40 nm core diameter) with various shell thicknesses as indicated in the figure. (D) Calculated near-field distributions of (i) Ag nanosphere (40 nm diameter, 405 nm excitation) and Ag−Cu_2O core−shell nanoparticles of (ii) 4 nm shell thickness a t 505 nm excitation, (iii) 10 nm shell thickness at 578 nm excitation, (iv) 20 nm shell thickness at 635 nm excitation, and (v) 40 nm shell thickness at 686 nm excitation. (E) Maximum near-field enhancement ($|E_{max}/E_0|^2$) on the Ag and Cu_2O surfaces as a function of shell thickness (40 nm core) upon dipole plasmon excitations. (F) Experimental extinction spectra of Ag quasi-spherical nanoparticles (100 nm average diameter) and Ag−Cu_2O core−shell nanoparticles with various shell thicknesses obtained upon the addition of different volumes of 100 mM $Cu(NO_3)_2$ as indicated in the figure. (G) Calculated extinction spectra of Ag−Cu_2O core−shell nanospheres (100 nm core diameter) with various shell thicknesses as indicated in the figure. (H) Calculated near-field distributions of Ag nanosphere (100 nm in diameter) at (i) 498 nm and (ii) 403 nm excitations and Ag−Cu_2O core−shell nanosphere (100 nm core diameter, 30 nm shell thickness) at (iii) 757 nm and (iv) 628 nm excitations. (I) Maximum near-field enhancement ($|E_{max}/E_0|^2$) on the Ag and Cu_2O surfaces as a function of shell thickness (100 nm core) upon dipolar and quadrupolar plasmon excitations.

dx.doi.org/10.1021/jp5064116 | J. Phys. Chem. C 2014, 118, 19948−19963

demonstrated that the epitaxial overgrowth of Cu_2O on Au nanoparticles also occurred under similar experimental conditions.[50] The epitaxial growth of Cu_2O on Ag quasi-spherical nanoparticles resulted in the formation of Ag−Cu_2O concentric core−shell nanoparticles (Figure 1B−D). The thickness of Cu_2O shells could be fine-controlled in the range from ∼3 nm to ∼50 nm by simply altering the molar ratio of $Cu(NO_3)_2$ to the Ag cores and the quasi-spherical morphology was well-preserved throughout the entire shell thickness tuning range. The as-fabricated Ag−Cu_2O core−shell nanoparticles exhibited rough outer surfaces textured with nanoscale features, as shown in the TEM (Figure 1B−D) and SEM (Figure 1E) images. EDS analysis (Figure 1F) showed the presence of Ag, Cu, and O in the core−shell nanoparticles and the results of the EDS line-scan elemental mapping (Figure 1G) obtained on an individual particle further verified the well-defined Ag core-Cu_2O shell heterostructure.

HRTEM measurements provided detailed structural information on the Ag core, the Cu_2O shell, and the interfaces between the core and the shell. As shown in Figure 1H, the Ag quasi-spherical core had multitwined crystalline structures with clearly resolved boundaries between different crystalline domains and the Ag surfaces were enclosed by multiple thermodynamically stable low-index facets, such as {111} and {100} facets, oriented along different directions. The surfaces of the Ag core were composed of atomically well-defined crystalline facets, each of which served as a locally flat substrate for the epitaxial growth of a Cu_2O monocrystalline layer. As the Cu_2O layers grew thicker, they coalesced with each other to evolve into a continuous shell with nanoscale protrusions or grooves formed at the crystalline boundaries, giving rise to the surface roughness of the core−shell particles. As shown in HRTEM image (Figure 1H) and the corresponding Fast Fourier Transform (FFT) pattern (inset of Figure 1H), the Cu_2O shell was composed of a number of Cu_2O crystalline domains with various orientations. Moiré patterns,[13,29,72,73] which appeared as fringes composed of alternating bright and dark stripes in the HRTEM image, were clearly observed as a result of the superposition of the two mismatched crystalline lattices of Ag and Cu_2O. The regions 1 and 2 labeled in Figure 1H were further zoomed in as Figure 1I and J, respectively. The lattice fringes had *d* spacings of 0.24 and 0.23 nm corresponding to the (111) planes of Cu_2O and Ag, respectively. The epitaxial growth of the Cu_2O shell at the Ag−Cu_2O interfaces was clearly observed in the HRTEM images. The FFT patterns of the Cu_2O shell regions (upper right panels of Figure 1I and J) and the Ag core regions (lower right panels of Figure 1I and J) showed excellent alignment of the crystalline orientations, further verifying the epitaxial growth of the Cu_2O shells on the Ag cores.

The plasmon resonance of the Ag−Cu_2O core−shell nanoparticles (40 nm quasi-spherical core) could be fine-tuned across the entire visible spectral region by adjusting the thickness of the Cu_2O shells, giving rise to a diverse range of colors of the colloidal particles (Figure 2A). The color evolution of the colloidal suspensions, which could be observed in real time, provided an extremely straightforward way to monitor the shell growth process (Figure S2 in Supporting Information). The experimental extinction (absorption + scattering) spectra of colloidal Ag−Cu_2O core−shell nanoparticles with core size of 40 nm and various shell thicknesses are shown in Figure 2B. The bared Ag quasi-spherical nanoparticles (black curve in Figure 2B) exhibited a characteristic dipole plasmon resonance peak at ∼410 nm, which progressively red-shifted as the Cu_2O shell thickness increased due to the large refractive index of the Cu_2O shell. The spectral red-shifts of plasmon resonances upon increase in shell thickness have also been observed in several other metal−semiconductor core−shell nanoparticles.[36,39,43] Meanwhile, additional spectral features below 500 nm gradually developed as the Cu_2O shell thickness increased. These spectral features were attributed to the geometry-dependent optical characteristics of Cu_2O nanoshells as discussed in detail in our previous publications.[38,50,74−76] To gain more quantitative insights into the geometry-dependence of the optical properties, we used the FDTD method to calculate the far-field extinction and near-field enhancements of spherically symmetric Ag−Cu_2O core−shell nanoparticles with fixed core diameter of 40 nm and varying shell thicknesses. As shown in Figure 2C, both the plasmon resonance frequencies and spectral line shapes of the calculated extinction spectra were in very good agreement with the experimental results. Figure 2D shows the calculated near-field distributions of the Ag−Cu_2O core−shell nanospheres with various shell thicknesses upon the excitation of the dipole plasmon resonance. The calculated maximum field enhancements ($|E/E_0|^2$) on the Ag core surface and the Cu_2O shell surface were plotted as a function of the Cu_2O shell thickness in Figure 2E. The shell-thickness-dependent evolution of near-field enhancements can be interpreted in the context of both field confinement and plasmon damping effects introduced by the Cu_2O shell. When the Ag core was encapsulated in a Cu_2O nanoshell thinner than 10 nm, the field enhancements on the Ag surface significantly decreased and extended from the Ag core across the Cu_2O shell all the way to the outer surface of the core−shell particles. Increasing the shell thickness resulted in better spatial confinement of the near-field enhancements, and the electric field was mostly enhanced on the surface of the Ag core with negligible enhancements on the outer surface of the Cu_2O shell when the shell became thicker than 30 nm. In the thin shell regime, the plasmon resonance was in the spectral region above the band gap of Cu_2O and was thus significantly damped due to the interband transitions of the Cu_2O shells.[50] As the shell thickness increased, the plasmon resonance was further shifted to longer wavelengths where the Cu_2O shell behaved as a dielectric layer, resulting in less plasmon damping and consequently higher field enhancements on the Ag surface. As shown in Figure S3 in Supporting Information, the overall extinction of the 40 nm Ag nanosphere at the plasmon resonance wavelength had ∼60% contribution from absorption and ∼40% contribution from scattering. Coating the Ag core with a Cu_2O nanoshell significantly increased the relative ratios of absorption to scattering cross sections. As a result, the overall extinction of the Ag−Cu_2O core−shell nanospheres was dominated by absorption, and such wavelength-tunable light absorption gave rise to the vivid colors of the colloidal particles shown in Figure 2A.

Cu_2O nanoshells with fine-controlled thicknesses could also be grown on larger Ag quasi-spherical cores (average diameter of 100 nm) through the same epitaxial growth process (see Figure S4 in Supporting Information). As shown in Figure 2F, these larger Ag nanoparticles exhibited a dipole plasmon resonance shifted to ∼520 nm and a sharp quadrupole plasmon resonance peak at ∼410 nm in the extinction spectrum. The emergence of the quadrupole resonance and the broadening of the dipole resonance peak for the 100 nm Ag nanoparticles was essentially a consequence of phase retardation effects.[58,77−79]

dx.doi.org/10.1021/jp5064116 | J. Phys. Chem. C 2014, 118, 19948−19963

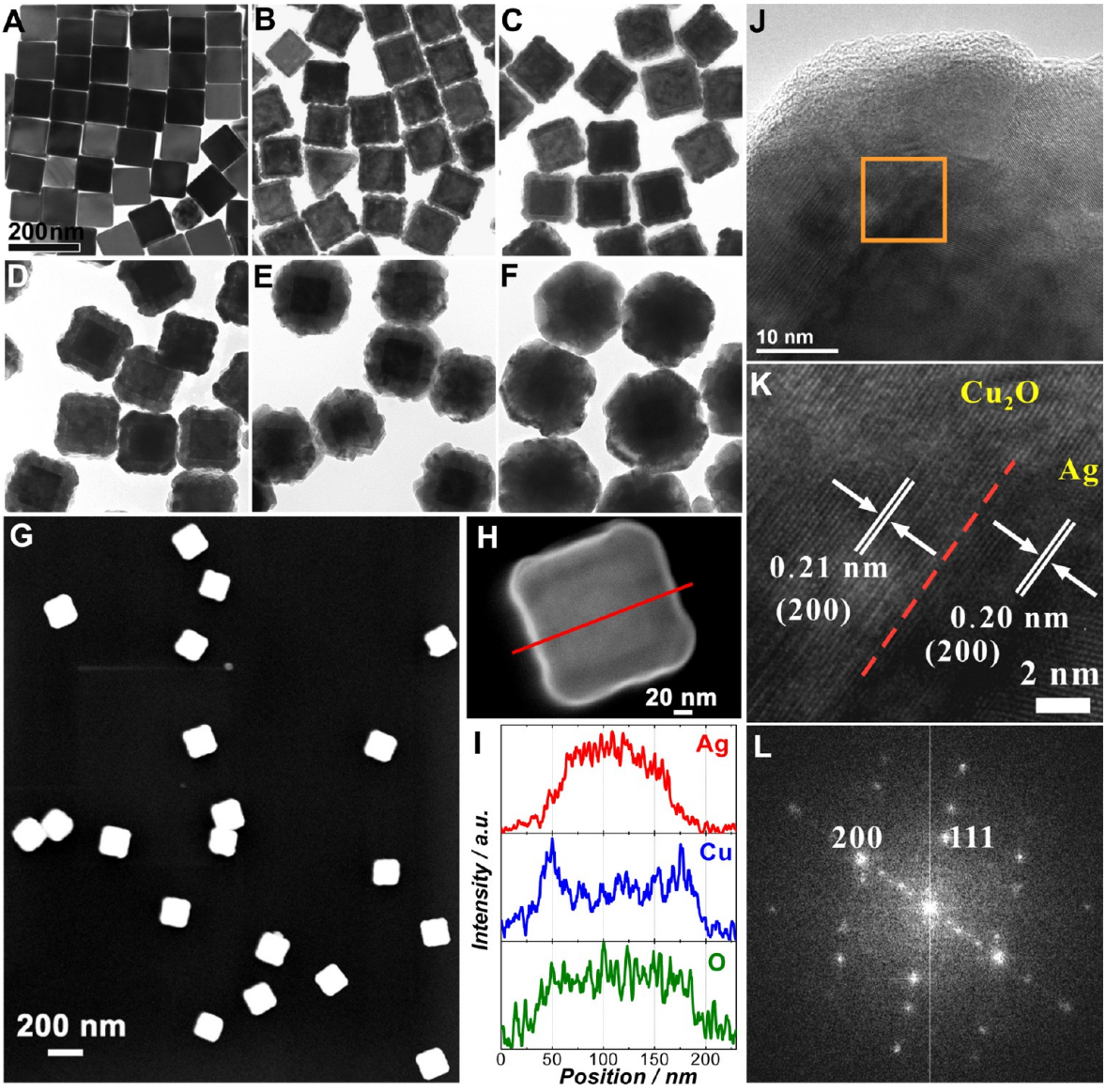

Figure 3. Growth of Cu_2O nanoshells on 100 nm Ag nanocube cores. TEM images of (A) Ag nanocubes (100 nm in edge length) and Ag−Cu_2O core−shell nanoparticles with various shell thicknesses obtained by adding (B) 10 μL, (C) 20 μL, (D) 60 μL, (E) 100 μL, and (F) 150 μL of 100 mM $Cu(NO_3)_2$ solution. All TEM images share the same scale bar in panel A. (G, H) SEM images of Ag−Cu_2O core−shell nanocubes from the sample shown in panel D. (I) Spatial elemental distribution obtained from the EDS line scan measurements along the red line shown in panel H based on the L-lines of Ag and K-lines of Cu and O. (J) HRTEM image of one corner of an individual Ag−Cu_2O core−shell nanocube. The particle were imaged with projection from the [001] zone axis. (K) Zoom-in image of the region highlighted in panel J. The red dash line highlights the boundary between the Ag and Cu_2O. (L) FFT pattern obtained from panel K.

Increasing the Cu_2O shell thickness led to progressive red-shift of both the dipole and quadrupole plasmon resonances. As Cu_2O shell thickness increased, the dipole plasmon resonance remained robust while the quadrupole plasmon feature became weaker and less distinctive, making the overall extinction more dipolar in nature. The damping of the quadrupole resonance was more significant than the dipole resonance largely due to the fact that the quadrupole resonance was in the spectral region overlapping with the interband transitions of Cu_2O. Precise control over the core and shell geometry of these highly monodisperse and uniform core−shell nanoparticles enabled us to achieve excellent match between the experimentally measured (Figure 2F) and FDTD-calculated extinction spectra (Figure 2G). In contrast to the core−shell nanoparticles with 40 nm Ag cores, the increase in the core size significantly increased the scattering cross sections of the particles. Therefore, the extinction spectral features of the core−shell nanoparticles with 100 nm Ag cores were dominated by scattering rather than absorption (Figure S5 in Supporting Information). Increasing the Cu_2O shell thickness led to the amplification of the scattering cross sections at the plasmon resonance wavelengths. Figure 2H shows the calculated near-field distributions of a 100 nm Ag nanosphere and a Ag−Cu_2O core−shell particles with core diameter of 100 nm and shell thickness of 30 nm. Similar to the core−shell nanoparticles with 40 nm Ag cores, the near-field enhancements became more confined on the Ag core surface as the shell thickness increased (Figure 2I). However, the plasmonic near-field enhancements of these larger particles extended over longer distances from the core than the particles with smaller Ag cores.

dx.doi.org/10.1021/jp5064116 | J. Phys. Chem. C 2014, 118, 19948−19963

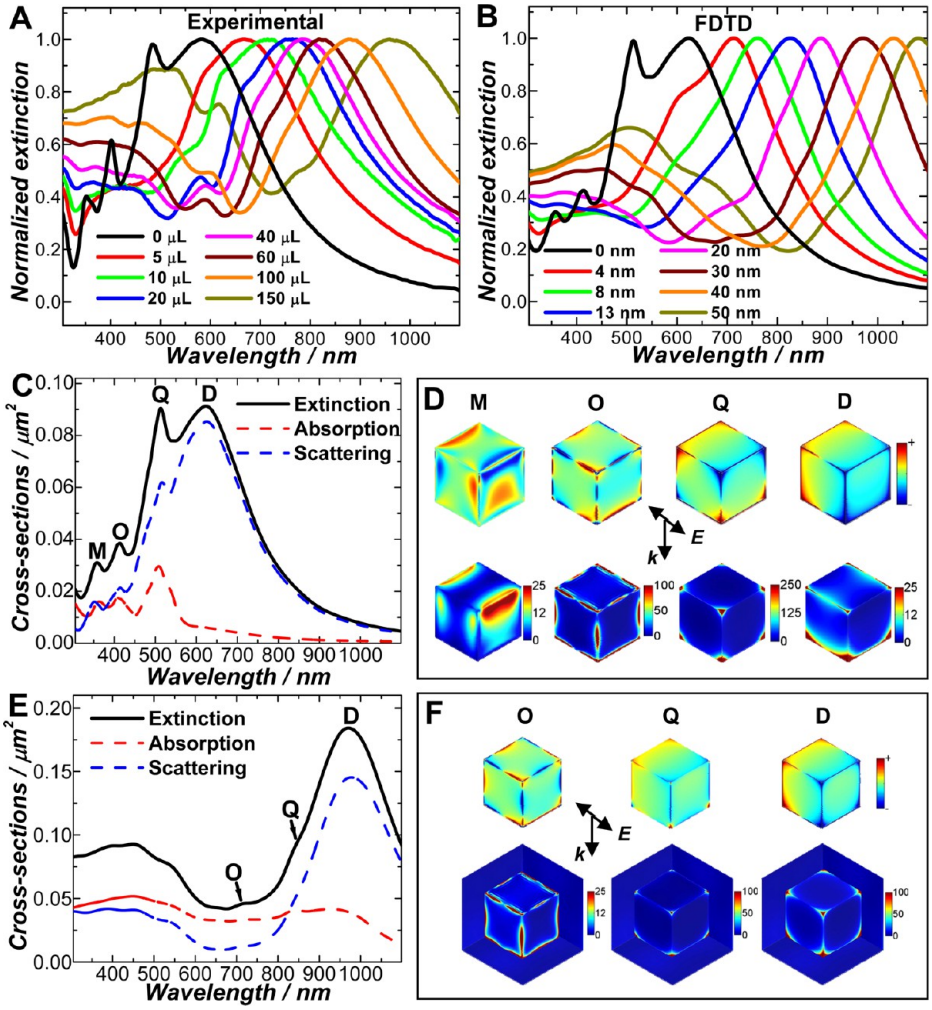

Figure 4. Tunable optical properties of Ag−Cu_2O core−shell nanocubes (100 nm nanocube core). (A) Experimental extinction spectra of Ag nanocubes and of Ag−Cu_2O core−shell nanoparticles with various shell thicknesses obtained upon the addition of different volumes of 100 mM $Cu(NO_3)_2$ solution. (B) Calculated extinction spectra of Ag−Cu_2O core−shell nanocubes with various shell thicknesses. (C) Calculated absorption, scattering, and extinction spectra of the Ag nanocube. (D) Calculated surface charge (top row) and near-field (bottom row) distributions of the Ag nanocube at 355, 420, 544, and 632 nm excitations, from left to right. (E) Calculated absorption, scattering, and extinction spectra of the Ag−Cu_2O core−shell nanocube with shell thickness of 30 nm. (F) Calculated surface charge (top row) and near-field (bottom row) distributions of the Ag−Cu_2O core−shell nanocube at 690, 800, and 964 nm excitations, from left to right. The dipole, quadrupole, octupole, and even higher-order multipole resonances are labeled as D, Q, O and M, respectively. The incidence and polarization direction of the excitation are illustrated in each panel.

Ag−Cu_2O Core−Shell Nanoparticles with Nanocube Cores. In contrast to the Ag quasi-spherical nanoparticles, Ag nanocubes are single-crystalline in nature with well-defined flat surfaces, making them an ideal core material for the epitaxial shell growth to form conformal core−shell nanostructures. We followed the protocol developed by Xia and co-workers[65] to fabricate Ag nanocubes with fine-controlled edge lengths in the range from ∼40 nm to ∼150 nm. As shown in Figure 3A, the as-fabricated Ag nanocubes were highly monodisperse with edge lengths of 100 nm ±3.8 nm and exhibited uniform cubic morphology with slight truncations at the corners. The expitaxial growth of Cu_2O on the Ag nanocubes occurred under similar conditions as the growth on the quasi-spherical cores. The thickness of Cu_2O shells could be fine-controlled in the range of ∼4 nm to ∼80 nm by adjusting the ratios of $Cu(NO_3)_2$ to the Ag nanocubes (Figure 3B−H). The cubic shape of the core−shell nanoparticles was well-preserved in the thin shell regime; however, significant corner truncations started to develop as the Cu_2O shell thickness further increased to beyond ∼50 nm and the core−shell particles gradually evolved into a cubooctahedral morphology. The EDS line-scan analysis (Figure 3I) verified the well-defined core−shell structures of the particles. The epitaxial growth of the Cu_2O shell on the {100} facets of the Ag nanocube core was clearly observed in the HRTEM images (Figure 3J and K). FFT pattern of the image in Figure 3K further confirmed the epitaxial growth of Cu_2O along the [100] direction (Figure 3L).

The 100 nm Ag nanocubes exhibited much richer plasmonic features in the extinction spectrum than the 100 nm Ag quasi-spherical nanoparticles. As shown in the black curve in Figure 4A, the Ag nanocubes displayed four distinct plasmon peaks at 590, 490, 410, and 360 nm, respectively. The FDTD-calculated extinction spectrum of a Ag nanocube with edge length of 100 nm (the black curve in Figure 4B) also exhibited four distinct plasmon resonances with peak positions and line shapes in excellent agreement with those experimentally observed. According to previously reported discrete dipole approximation (DDA) calculation results,[61,80,81] these four extinction peaks

dx.doi.org/10.1021/jp5064116 | J. Phys. Chem. C 2014, 118, 19948−19963

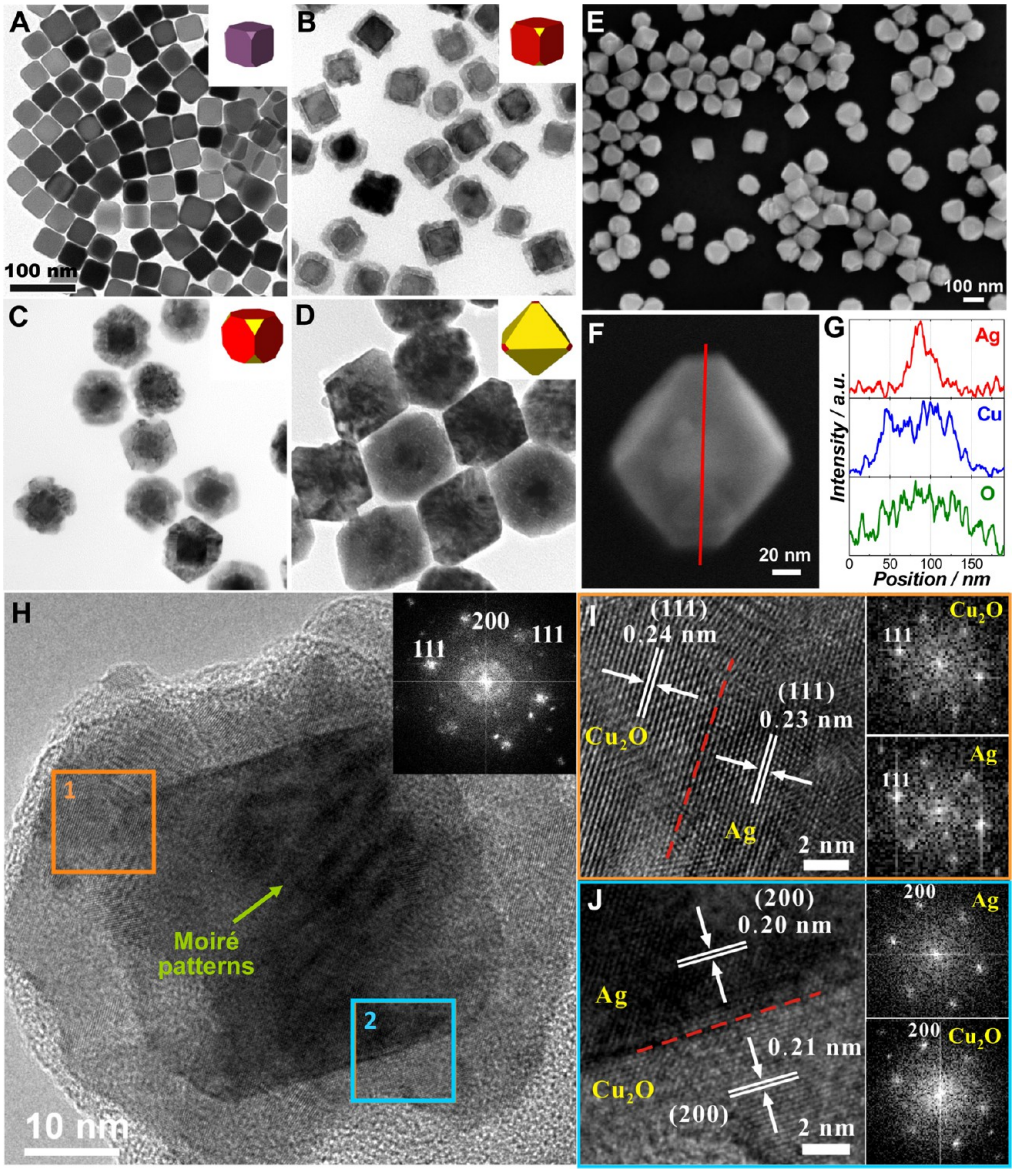

Figure 5. Growth of Cu_2O nanoshells on truncated Ag nanocubes (40 nm in edge length). TEM images of (A) truncated Ag nanocubes and Ag−Cu_2O core−shell nanoparticles with various shell thicknesses obtained by adding (B) 10 μL, (C) 30 μL, and (D) 100 μL of 100 mM $Cu(NO_3)_2$ solution. All TEM images share the same scale bar in panel A. The inset shows schematic illustration of structures from truncated Ag nanocubes to truncated core−shell nanocubes and truncated octahedra as Cu_2O shell thickness increases. (E, F) SEM images of Ag−Cu_2O nanoparticles selected from panel D. (G) Spatial elemental distribution obtained from the EDS line scan measurements along the red line shown in panel F based on the L-lines of Ag and K- lines of Cu and O. (H) HRTEM image of an individual Ag−Cu_2O core−shell nanoparticle. The particle were imaged with projection from the [011] zone axis. The top-right inset is the Fourier transform pattern of the region encompassing the whole cross section of the core−shell particle. (I, J) HRTEM images showing the Au−Cu_2O interfacial structures a n d the corresponding FFT patterns of regions 1 and 2 in panel H, respectively. The red dash lines highlight the boundary between the Ag and Cu_2O. The right panels of Figure I and J show the FFT patterns of the Ag core and Cu_2O shell regions.

were assigned to the dipole, quadrupole, and arguably higher-order plasmon modes, respectively, in the order from longer to shorter wavelengths. As the thickness of the Cu_2O shell increased, all the four plasmon peaks progressively shifted to longer wavelengths (Figure 4A). In striking contrast to the highly robust dipole plasmon peak, the higher-order modes showed significantly decreased extinction cross sections upon increase in the shell thickness and gradually evolved into weak spectral features either as shoulders of the dipole resonance peak or on top of the scattering background from the Cu_2O nanoshells. The calculated extinction spectra of Ag−Cu_2O core−shell nanocubes (Figure 4B) showed quantitative agreement with the experimental results in terms of both the plasmon shift and spectral line-shape evolution. The Ag−Cu_2O core−shell nanocubes exhibited plasmonic tunability over a broader spectral range than the Ag−Cu_2O core−shell nanospheres of similar core sizes and shell thicknesses due to the fact that the nanocube plasmon resonances are more sensitive to the refractive index of the surrounding medium than the nanosphere plasmons.[59,82,83]

In Figure 4C, the calculated extinction spectrum of a 100 nm Ag nanocube was further decomposed into scattering and absorption contributions. Because of the relatively large particle size, the extinction spectral features were dominated by

dx.doi.org/10.1021/jp5064116 | J. Phys. Chem. C 2014, 118, 19948−19963

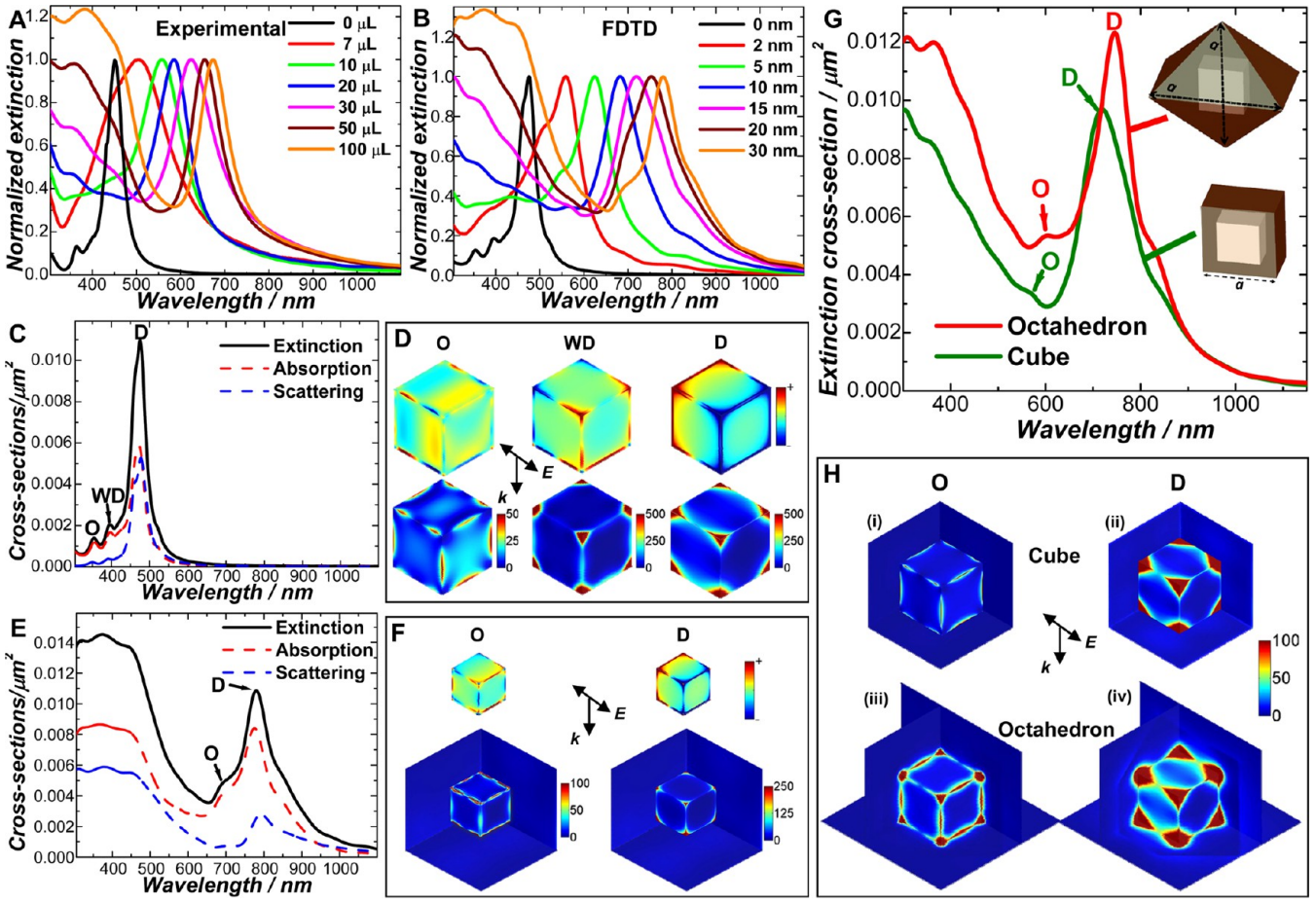

Figure 6. Tunable optical properties of Ag−Cu_2O core−shell nanoparticles with 40 nm nanocube cores. (A) Experimental extinction spectra of truncated Ag nanocubes and of Ag−Cu_2O core−shell nanoparticles with various shell thicknesses obtained upon the addition of different volumes of 100 mM $Cu(NO_3)_2$ solution. (B) Calculated extinction spectra of Ag−Cu_2O core−shell nanocubes with various shell thicknesses. (C) Calculated absorption, scattering, and extinction spectra of the Ag nanocube. (D) Calculated surface charge (top row) and near-field (bottom row) distributions of the Ag nanocube at 362, 412, and 485 nm excitations, from left to right. (E) Calculated absorption, scattering, and extinction spectra of a Ag−Cu_2O core−shell nanocube with shell thickness of 30 nm. (F) Calculated surface charge (top row) and near-field (bottom row) distributions of Ag−Cu_2O core−shell nanoparticle with the shell thickness of 30 nm at the resonance peaks of 695 and 785 nm, from left to right. The dipole, weak dipole, and octupole resonances are labeled as D, WD, and O, respectively. (G) Calculated extinction spectra of a Ag−Cu_2O core−shell nanocube (a = 70 nm) and a core−shell octahedral particle (a = 120 nm). Both particles have a Ag nanocube core with edge length of 40 nm. The insets show the schematic illustration of the structures of the cubic and octahedral nanoparticles. (H) Calculated near-field enhancements of cubic core−shell particle at 564 and 718 nm excitations (top row) and of the octahedral core−shell particle at 605 and 746 nm excitations (bottom row). The dipole and octupole resonances are labeled as D and O, respectively.

scattering with small contribution from absorption. The calculated surface charge and near-field distributions upon excitation of different plasmon modes (Figure 4D) allowed us to assign the four extinction peaks to the dipole, quadrupole, octupole, and higher-order multipole plasmon resonances, which were labeled as D, Q, O, and M respectively in Figure 4C and D. Although the 100 nm Ag nanocube had similar extinction cross sections at the dipole and quadrupole resonance wavelengths, the maximum field enhancement ($|E_{max}/E_0|^2$) associated with the quadrupole resonance excitation was much higher than that of the dipole resonance excitation. Interestingly, the field enhancement achievable upon the octupole resonance excitation was also significantly higher than the dipole resonance, though the octupole mode had much smaller extinction cross section. The octupole resonance of the Ag nanocube was previously identified through DDA calculations as a novel large field enhancement but low extinction (LFE-LE) mode,[61,80] which was further confirmed here by our FDTD calculations. The origin of this LFE-LE mode, which could be interpreted as a synergistic consequence of confinement of high density of charges and energy flux in a tiny volume around the nanocube edges and corners, was discussed in detail in a previously published work.[80]

Figure 4E shows the calculated extinction, absorption, and scattering spectra of a Ag−Cu_2O core−shell nanocube with core edge length of 100 nm and shell thickness of 30 nm. The dipole, quadrupole, and octupole resonance peaks were all significantly red-shifted due to the large refractive index of the Cu_2O shell. The dipole extinction peak, which was dominated by scattering, remained robust, while the quadrupole and octupole exhibited very small cross sections and thus, became much less distinguishable. Therefore, the extinction spectral features of the core−shell nanocube became more dipolar in nature than those of the bare Ag core in spite of the increase in the overall particle size. Different from the core−shell nanospheres, the plasmon field enhancements of the core−shell nanocube was strictly confined in close proximity to the surface of the Ag core with negligible extension into the Cu_2O

dx.doi.org/10.1021/jp5064116 | J. Phys. Chem. C 2014, 118, 19948−19963

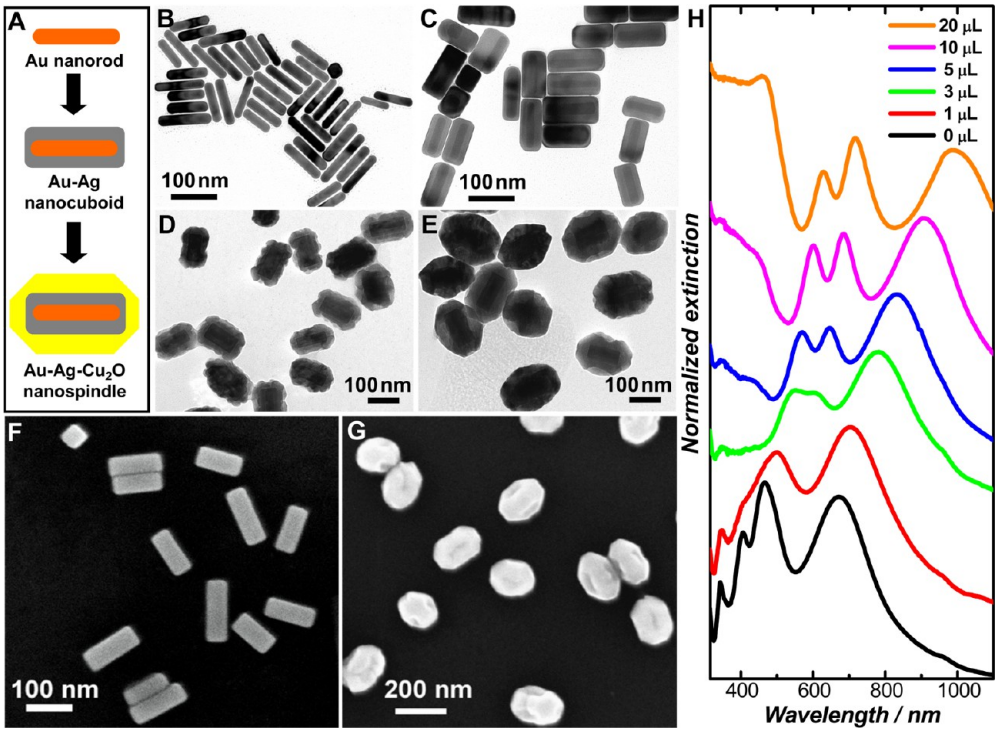

Figure 7. Growth of Cu_2O nanoshells on Au−Ag core−shell nanocuboids. (A) Schematic illustration of the structural evolution from cylindrical Au nanorods to Au−Ag truncated nanocuboids to the Au−Ag−Cu_2O triple- layered nanospindles. TEM images of (B) Au nanorods, (C) Au−Ag core−shell nanocuboids, and Au−Ag−Cu_2O triple-layered nanoparticles with different shell thicknesses obtained by adding (D) 10 μL and (E) 20 μL of 100 mM $Cu(NO_3)_2$ solution. SEM images of (F) Au−Ag core−shell nanocuboids and (G) Au−Ag−Cu_2O triple- layered nanospindles. (H) Experimental extinction spectra of Au−Ag nanocuboids (black curve) and Au−Ag- Cu_2O triple-layered nanoparticles obtained by adding different volumes of 100 mM $Cu(NO_3)_2$ solution as labeled in the figure.

shell. The maximum field enhancements for the both the quadrupole and octupole resonances significantly went down when the Ag nanocube was encapsulated in the Cu_2O shell, nevertheless, the maximum field enhancements associated with the dipole resonance increased possibly due to the tighter confinement of charges and energy flux on the Ag surfaces by the Cu_2O shell.

We also used smaller Ag nanocubes (edge lengths of 40 ± 2.8 nm) as the core materials to fabricate the Ag−Cu_2O core−shell nanoparticles. In comparison to the 100 nm Ag nanocubes with relatively sharp corners, these smaller nanocubes exhibited a truncated cubic morphology in the TEM image (Figure 5A). These truncated nanocubes were enclosed by {100} facets on the sides and {111} facets exposed at the corners. During the epitaxial growth of Cu_2O, the morphology of core−shell nanoparticles evolved gradually from the original truncated nanocubes to cubooctahedra and eventually to slightly truncated octahedra as the corner truncations became increasingly significant (Figure 5B−F). The Ag core−Cu_2O shell structure of the truncated octahedral nanoparticles was verified by EDS line-scan measurements shown in Figure 5G. Such shape evolution could be interpreted as a result of the competition between the epitaxial growth of Cu_2O on the Ag {100} and the Ag {111} facets. The epitaxial growth of Cu_2O along both the [111] and [100] directions on the 40 nm Ag nanocube core was confirmed by the HRTEM images and the FFT patterns shown in Figure 5H−J. Because the {111} facet has lower surface energy than the {100} facet of Cu_2O,[84] the shell growth along [100] direction was faster than that along the [111] direction. Therefore, as the Cu_2O grew thicker, the outer surfaces of the core−shell nanoparticles became more dominated by the {111} rather than the {100} facets.

In contrast to the 100 nm Ag nanocubes with four distinct plamson resonances, the experimental extinction spectra of the 40 nm nanocubes were dominated by a sharp peak at ∼425 nm with two small shoulders at ∼400 nm and ∼360 nm, respectively (black curve in Figure 6A). As the Cu_2O shell thickness increased, the major extinction peak was observed to experience progressive red-shift from ∼425 nm to almost 700 nm while additional characteristic spectral features of the Cu_2O shell gradually developed in the shorter wavelength region. To gain more quantitative insights on how the Cu_2O shell modulated the various plasmon modes of the Ag core, FDTD was used to calculate the extinction spectra of core−shell nanocubes with a 40 Ag nanocube core and a Cu_2O shell of varying thickness (Figure 6B). The shell thickness dependent extinction peak shift and spectral line-shape evolution were both in good agreement with the experimental observations. As shown in Figure 6C, absorption and scattering had almost equal contribution to the major extinction peak of the 40 nm Ag nanocube, while the two small spectral shoulders on the blue side of the major peak were dominated by absorption. Based on the surface charge and near-field distributions calculated by FDTD (Figure 6D), we were able to assign the major extinction peak and the two spectral shoulders to a dipole, a weak dipole, and an octupole plasmon mode, which were labeled as D, WD, and O respectively in Figure 6C. The quadrupole mode of the nanocube might be optically dark, and thus was not observed in the extinction spectrum. The weak dipole exhibited a charge distribution pattern that was oriented oppositely to that of the dipole resonance. More interestingly,

dx.doi.org/10.1021/jp5064116 | J. Phys. Chem. C 2014, 118, 19948−19963

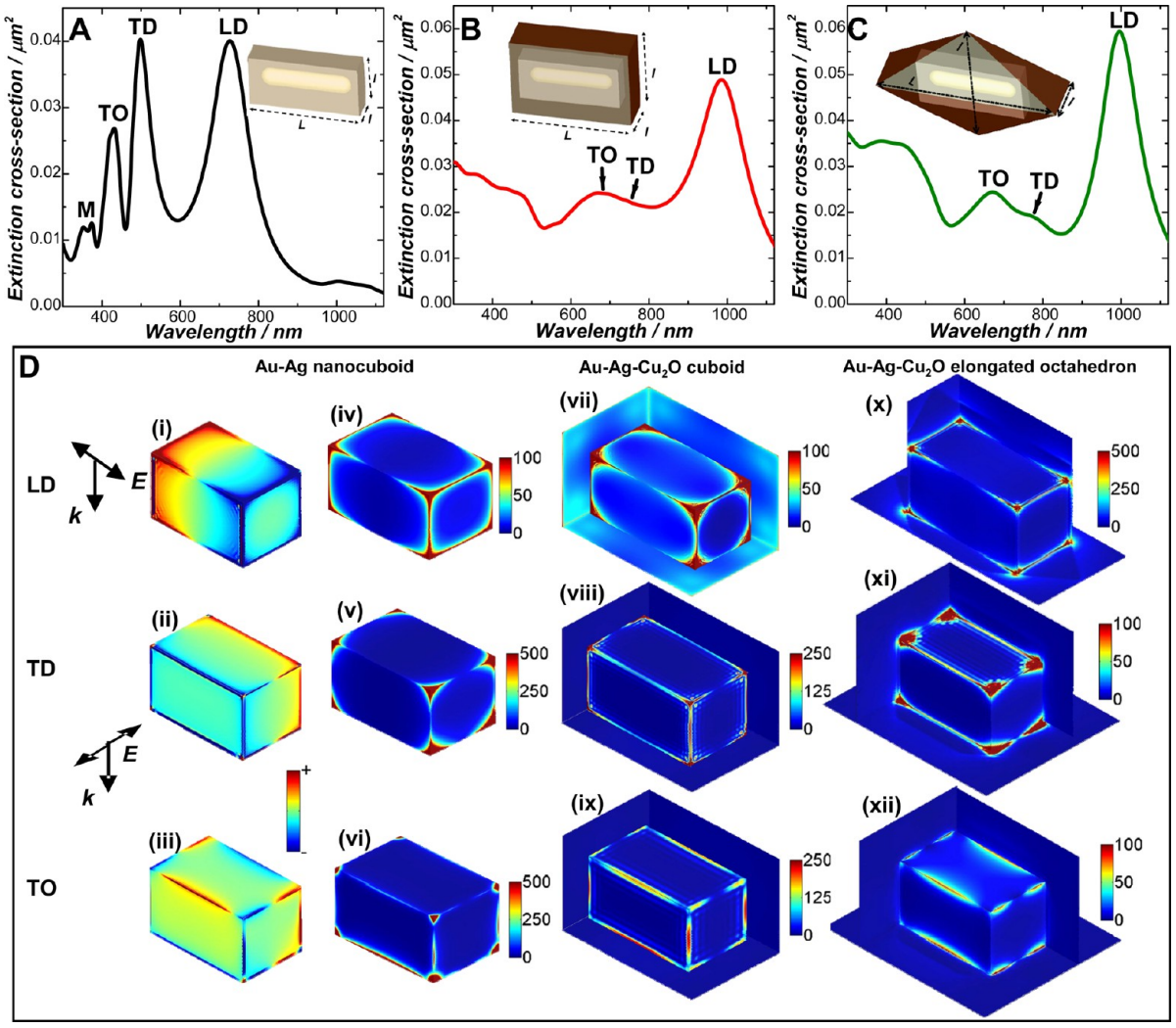

Figure 8. Calculated far-field and near-field properties of core−shell nanoparticles with a cuboidal core. Calculated extinction spectra of (A) Au−Ag nanocuboid (L = 110 nm, l = 50 nm), (B) Au−Ag−Cu_2O cuboid with 13 nm Cu_2O shell thickness (L = 136 nm, l = 76 nm), and (C) Au−Ag−Cu_2O triple-layered elongated octahedron (L = 190 nm, l = 130 nm). (D) Calculated surface charge (left-most column) and near-field enhancement distribution (the second column from the left) of Au−Ag nanocuboid at 727 nm (i, iv), 495 nm (ii, v), and 431 nm (iii, vi) excitations. Calculated near-field enhancement distribution (the third column from the left) of Au−Ag−Cu_2O cuboid at 996 nm (vii), 745 nm (viii), and 671 nm (ix) excitations. Calculated near-field enhancement distribution (right-most column) of Au−Ag−Cu_2O elongated octahedron at 998 nm (x), 771 nm (xi), and 665 nm (xii) excitations. Longitudinal dipole, transverse dipole, transverse octupole, and higher-order multipole resonances are labeled as LD, TD, TO and M, respectively.

the weak dipole mode showed near-field intensities similar to those of the dipole , though its extinction cross section was much smaller than the dipole mode. This weak dipole mode was another LFE-LE resonance mode that has never been identified before.[85] For the core−shell nanocube with 30 nm thick Cu_2O shell, the dipole and octupole resonances both significantly red-shifted while the weak dipole peak became indistinguishable in the extinction spectrum (see Figure 6E). As shown in Figure S6 in Supporting Information, the colloidal core−shell nanoparticles fabricated using the 40 nm nanocubes as the core displayed a diverse set of colors because their major extinction peaks were dominated by absorption rather than scattering (Figure 6E). The calculated near-field distributions of the core−shell nanocube (Figure 6F) showed that the field enhancements were largely confined on the surface of the Ag core, similar to those of the larger Ag−Cu_2O core−shell nanocube shown in Figure 4F.

We further evaluated the effects of shell morphologies on the far-field and near-field optical properties of the core−shell nanoparticles through FDTD calculations. In Figure 6G, we compare the calculated extinction spectra of a Ag−Cu_2O core−shell nanocube (edge length of 70 nm) and a core−shell octahedral particle (edge length of 120 nm). Both particles had a Ag nanocube core with edge length of 40 nm and approximately the same total volume of Cu_2O in the shell. The core−shell nanooctahedron exhibited further red-shifted dipole and octupole plasmon resonances than the core−shell nanocube. The dipole resonance peak of the core−shell nanooctahedron had a narrower bandwidth and was more intense than that of the core−shell nanocube. The near-field enhancements of both particles at the dipole resonance wavelength were much higher than at the octupole resonance wavelength (Figure 6H). The nanooctahedron exhibited higher field enhancement than the nanocube upon octupole plasmon excitation, whereas the dipole plasmon field enhancements

dx.doi.org/10.1021/jp5064116 | J. Phys. Chem. C 2014, 118, 19948−19963

were comparable for both particles. The near-field distributions of the core−shell octahedron extended out from the Ag core surfaces into the Cu_2O shell, an interesting feature distinct from the core−shell nanocube whose field enhancements were well-confined on the Ag core surfaces.

Au−Ag−Cu_2O Triple-Layer Nanoparticles with Nanocuboid Cores. Cu_2O shells could also be grown epitaxially on the surfaces of Ag nanocuboids to form geometrically more complicated, anisotropic core−shell nanostructures. While Ag nanospheres and nanocubes represent two geometrically symmetric nanostructures, Ag nanocuboids are elongated, anisotropic nanoparticles with polarization-dependent responses to the incident light, exhibiting both transverse and longitudinal plasmon resonances. Controlled growth of Cu_2O nanoshells on Ag nanocuboid cores allowed us to systematically study how the semiconducting shell introduces interesting modifications to the different plasmon modes of the anisotropic cores. As illustrated in Figure 7A, we used single-crystalline Au nanorods as the core materials (see TEM image in Figure 7B), on which Ag nanoshells were then epitaxially grown to form Au−Ag core−shell nanocuboids.[67] Cetyltrimethylammonium chloride (CTAC) was used as a surface-capping ligand that selectively stabilized the {100} facets of Ag,[19,86] resulting in the formation of Au−Ag core−shell nanocuboids whose surfaces were dominated by {100} facets.[19,67,86] The as-fabricated nanocuboids showed intrinsic corner truncations with {111} facets exposed at the corners (see Figure 7C and F). During the epitaxial growth of Cu_2O, the nanoparticles underwent a morphological evolution from truncated nanocuboids into spindle-shaped particles as the Cu_2O shell thickness increased (Figure 7D, E, and G). EDS line-scan measurements on an individual nanospindle further confirmed the Au−Ag−Cu_2O triple-layer heterostructure (Figure S7 in Supporting Information). Similar to the Cu_2O growth on truncated Ag nanocubes, this morphological evolution could also be interpreted as a result of the competition between the epitaxial growth of Cu_2O on the Ag {100} and the Ag {111} facets.

In the experimental extinction spectra of the colloidal Au−Ag core−shell nanocuboids (see black curve in Figure 7H, and Figure S8A in Supporting Information), four distinct plasmon peaks were observed at 798, 460, 404, and 342 nm, which were assigned to the longitudinal dipole, transverse dipole, and two transverse octupole resonances, respectively.[67,87] As demonstrated previously, the frequencies and relative intensities of these plasmon resonance modes were dominated by the characteristics of the Ag shell rather than the Au nanorod core and can be systematically tuned across the visible and near-infrared regions by controlling the aspect ratio of the nanocuboids.[19,67,86] As shown in Figure S8A in Supporting Information, the bare Au nanorods had an intense longitudinal plasmon band at 900 nm and a weak transverse plasmon band at 520 nm. We found that as the Ag shell thickness increased, the longitudinal plasmon resonance progressively blue-shifted while multiple peaks of the transverse plasmon modes developed and became more intense, which was in excellent agreements with previously reported observations.[67,87] The extinction spectral evolution could be interpreted as a consequence of the increase in the width of the nanocuboids due to the preferential epitaxial growth of Ag on the side facets of the Au nanorods rather than on the nanorod tips.[19,67,8] TEM images revealed that the Ag shells grown on the lateral sides of the Au nanorods were thicker than those on the ends (see Figure S8B and S8C in Supporting Information). Once the nanocuboids were encapsulated in Cu_2O nanoshells, all the longitudinal and transverse plasmonic features were well-resolved in the experimental extinction spectra with resonances progressively shifted to longer wavelengths as the shell thickness increased (Figure 7H).

To better understand the effects of the Cu_2O shell on the plasmon resonances of the anisotropic nanocuboid core, we calculated the extinction spectra of a Au−Ag core−shell nanocuboid (Figure 8A), a Au−Ag−Cu_2O triple-layer nanocuboid (Figure 8B), and a Au−Ag−Cu_2O triple-layer nanoparticle with a cuboidal metallic core encapsulated in an elongated octahedral Cu_2O shell (Figure 8C). The triple-layer nanocuboid and elongated octahedron had the same volume of Cu_2O surrounding the nanocuboid cores. The calculated surface-charge and near-field distribution associated with various plasmon modes of the particles are shown in Figure 8D, which enabled us to assign each extinction peak to a particular plasmon resonance mode based on its characteristic surface-charge and near-field distribution patterns. In the calculated extinction spectrum of the Au−Ag core−shell nanocuboid with width (l) of 50 nm and length (L) of 110 nm, three intense, well-defined plasmon resoances were observed, which were assigned, from long to short wavelengths, to the longitudinal dipole (LD), transverse dipole (TD), and transverse octupole (TO) plasmon modes, respectively. The extinction spectral features of the two dipole resonances, LD and TD, were dominated by scattering, whereas scattering and absorption contributed almost equally to the overall spectral line shape of the octupole resonance peak (Figure S9A in Supporting Information). In addition, there was a weak double-peaked spectral feature below 400 nm in the calculated extinction spectra, which could be assigned to two transverse plasmon modes composed of either higher-order multipole resonances or hybrid modes with mixed contributions from multiple plasmon resonances (Figure S9B in Supporting Information). This double-peaked feature was experimentally observed as an asymmetric extinction peak at ∼355 nm (black curve in Figure 7H). As observed for the previous geometries, the coating with Cu_2O shells led to significant red-shifts of all the longitudinal and transverse plasmon resonances (Figure 8B and C). The elongated octahedron exhibited a more intense and narrower longitudinal dipole resonance peak than the triple-layer nanocuboid. It is well-known that for anisotropic Au nanorods, the field enhancements associated with the longitudinal plasmon resonance are much higher than those of the transverse plasmon resonance. However, for the Au−Ag core−shell nanocuboid, significantly higher field enhancements were achieved upon the excitation of the transverse plasmon modes than the longitudinal dipole plasmon. Once the nanocuboid core was encapsulated inside a Cu_2O shell, the field enhancements for the longitudinal dipole plasmon increased while the transverse plasmon modes showed significant decrease in field enhancements. The cuboidal Cu_2O shell showed the capability to strictly confine the field enhancements on the surfaces of the metallic core, whereas the field enhancements extended from the core surface into the shell region when the Cu_2O shell was grown into the elongated octahedral morphology.

■ CONCLUSIONS

We have demonstrated that the epitaxial growth of Cu_2O on Ag allows for the tight control over the particle geometries and the fine-tuning of the optical properties of Ag−Cu_2O core−shell

dx.doi.org/10.1021/jp5064116 | J. Phys. Chem. C 2014, 118, 19948−19963

nanoparticles. Several Ag nanostructures, such as quasi-spherical nanoparticles, nanocubes, and nanocuboids, were used as the core materials to construct hybrid core−shell nanoparticles. Each of these core geometries has its own unique optical characteristics, exhibiting multiple plasmon resonances in the optical extinction spectra. Epitaxial overgrowth of Cu_2O nanoshells on the Ag cores introduces interesting modifications to both the resonance frequencies and spectral line shapes of the different plasmon modes of the Ag cores. The capabilities to fine-control both the core and the shell geometries enables us to fine-tune the light absorption and scattering properties of the core−shell nanoparticles over a broad spectral range across the visible and near-infrared. Quantitative understanding of the geometry-dependent far-field and near-field optical characteristics of the Ag−Cu_2O core−shell nanoparticles were obtained experimentally through extinction spectroscopic measurements and theoretically through FDTD calculations. The knowledge gained through this study provides important information that may guide the rational design and controlled fabrication of metal−semiconductor hybrid heteronanostructures with increasing geometric complexity and further enhanced optical tunability.

■ ASSOCIATED CONTENT

Supporting Information

Additional TEM images of Ag quasi-spherical nanoparticles, Au−Ag core−shell nanocuboids, and various Ag−Cu_2O core−shell nanoparticles, true-color pictures showing the color evolution of the colloids during the epitaxial growth of Cu_2O nanoshells on 40 nm Ag quasi-spherical nanoparticles, calculated extinction, absorption, and scattering cross sections of various Ag−Cu_2O core−shell nanoparticles, true-color picture of colloidal suspensions of Ag−Cu_2O core−shell nanoparticles with 40 nm Ag nanocube cores, extinction spectra of colloidal Au−Ag core−shell nanocuboids, and SEM image and EDS line-scan elemental mapping results of an individual Au−Ag−Cu_2O nanospindle. This material is available free of charge via the Internet at http://pubs.acs.org.

■ AUTHOR INFORMATION

Corresponding Author

*E-mail: wang344@mailbox.sc.edu (H.W.). Fax: 803-777-9521. Tel.: 803-777-2203.

Present Address

[⊥]Department of Chemistry, Northwestern University, Evanston, Illinois 60208, United States.

Author Contributions

[§]H.J. and N.L. contributed equally.

Notes

The authors declare no competing financial interest.

■ ACKNOWLEDGMENTS

H.W. acknowledges the support by a National Science Foundation Faculty Early Career Development Award (DMR-1253231). N.L. acknowledges support from the Robert A. Welch Foundation (C-1222) and the Cyberinfrastructure for Computational Research funded by National Science Foundation under Grant CNS-0821727. The authors thank Prof. Peter Nordlander of Rice University for insightful discussions, Dr. Douglas A. Blom of USC Nanocenter for HRTEM measurements, and the University of South Carolina Electron Microscopy Center for instrument use and technical assistance.

■ REFERENCES

(1) Reiss, P.; Protiere, M.; Li, L. Core/Shell Semiconductor Nanocrystals. *Small* **2009**, *5*, 154−168.

(2) Caruso, F. Nanoengineering of Particle Surfaces. *Adv. Mater.* **2001**, *13*, 11−22.

(3) Cortie, M. B.; McDonagh, A. M. Synthesis and Optical Properties of Hybrid and Alloy Plasmonic Nanoparticles. *Chem. Rev.* **2011**, *111*, 3713−3735.

(4) Jiang, R. B.; Li, B. X.; Fang, C. H.; Wang, J. F. Metal/Semiconductor Hybrid Nanostructures for Plasmon-Enhanced Applications. *Adv. Mater.* **2014**, DOI: 10.1002/adma.201400203.

(5) Tao, F.; Grass, M. E.; Zhang, Y. W.; Butcher, D. R.; Renzas, J. R.; Liu, Z.; Chung, J. Y.; Mun, B. S.; Salmeron, M.; Somorjai, G. A. Reaction-Driven Restructuring of Rh-Pd and Pt-Pd Core−Shell Nanoparticles. *Science* **2008**, *322*, 932−934.

(6) Zhang, J. T.; Tang, Y.; Lee, K.; Ouyang, M. Tailoring Light-Matter-Spin Interactions in Colloidal Hetero-Nanostructures. *Nature* **2010**, *466*, 91−95.

(7) Zhang, H.; Jin, M. S.; Xia, Y. N. Enhancing the Catalytic and Electrocatalytic Properties of Pt-Based Catalysts by Forming Bimetallic Nanocrystals with Pd. *Chem. Soc. Rev.* **2012**, *41*, 8035−8049.

(8) Peng, X. G.; Schlamp, M. C.; Kadavanich, A. V.; Alivisatos, A. P. Epitaxial Growth of Highly Luminescent CdSe/CdS Core/Shell Nanocrystals with Photostability and Electronic Accessibility. *J. Am. Chem. Soc.* **1997**, *119*, 7019−7029.

(9) Li, J. J.; Wang, Y. A.; Guo, W. Z.; Keay, J. C.; Mishima, T. D.; Johnson, M. B.; Peng, X. G. Large-Scale Synthesis of Nearly Monodisperse CdSe/CdS Core/Shell Nanocrystals Using Air-Stable Reagents via Successive Ion Layer Adsorption and Reaction. *J. Am. Chem. Soc.* **2003**, *125*, 12567−12575.

(10) Talapin, D. V.; Koeppe, R.; Gotzinger, S.; Kornowski, A.; Lupton, J. M.; Rogach, A. L.; Benson, O.; Feldmann, J.; Weller, H. Highly Emissive Colloidal CdSe/CdS Heterostructures of Mixed Dimensionality. *Nano Lett.* **2003**, *3*, 1677−1681.

(11) Chen, O.; Zhao, J.; Chauhan, V. P.; Cui, J.; Wong, C.; Harris, D. K.; Wei, H.; Han, H. S.; Fukumura, D.; Jain, R. K.; et al. Compact High-Quality CdSe-CdS Core−Shell Nanocrystals with Narrow Emission Linewidths and Suppressed Blinking. *Nat. Mater.* **2013**, *12*, 445−451.

(12) Cho, E. C.; Camargo, P. H. C.; Xia, Y. N. Synthesis and Characterization of Noble-Metal Nanostructures Containing Gold Nanorods in the Center. *Adv. Mater.* **2010**, *22*, 744−748.

(13) Fan, F. R.; Liu, D. Y.; Wu, Y. F.; Duan, S.; Xie, Z. X.; Jiang, Z. Y.; Tian, Z. Q. Epitaxial Growth of Heterogeneous Metal Nanocrystals: From Gold Nano-Octahedra to Palladium and Silver Nanocubes. *J. Am. Chem. Soc.* **2008**, *130*, 6949−6951.

(14) Sanchez-Iglesias, A.; Carbo-Argibay, E.; Glaria, A.; Rodriguez-Gonzalez, B.; Perez-Juste, J.; Pastoriza-Santos, I.; Liz-Marzan, L. M. Rapid Epitaxial Growth of Ag on Au Nanoparticles: From Au Nanorods to Core−Shell Au@Ag Octahedrons. *Chem.—Eur. J.* **2010**, *16*, 5558−5563.

(15) Gong, J. X.; Zhou, F.; Li, Z. Y.; Tang, Z. Y. Synthesis of Au@Ag Core−Shell Nanocubes Containing Varying Shaped Cores and Their Localized Surface Plasmon Resonances. *Langmuir* **2012**, *28*, 8959−8964.

(16) Park, G.; Seo, D.; Jung, J.; Ryu, S.; Song, H. Shape Evolution and Gram-Scale Synthesis of Gold@Silver Core−Shell Nanopolyhedrons. *J. Phys. Chem. C* **2011**, *115*, 9417−9423.

(17) Bai, T. L.; Sun, J. F.; Che, R. C.; Xu, L. N.; Yin, C. Y.; Guo, Z. R.; Gu, N. Controllable Preparation of Core−Shell Au−Ag Nanoshuttles with Improved Refractive Index Sensitivity and SERS Activity. *ACS Appl. Mater. Interfaces* **2014**, *6*, 3331−3340.

(18) Park, K.; Drummy, L. F.; Vaia, R. A. Ag Shell Morphology on Au Nanorod Core: Role of Ag Precursor Complex. *J. Mater. Chem.* **2011**, *21*, 15608−15618.

(19) Li, Q.; Jiang, R. B.; Ming, T.; Fang, C. H.; Wang, J. F. Crystalline Structure-Dependent Growth of Bimetallic Nanostructures. *Nanoscale* **2012**, *4*, 7070−7077.

(20) Habas, S. E.; Lee, H.; Radmilovic, V.; Somorjai, G. A.; Yang, P. Shaping Binary Metal Nanocrystals Through Epitaxial Seeded Growth. *Nat. Mater.* **2007**, *6*, 692−697.
(21) Lim, B.; Wang, J. G.; Camargo, P. H. C.; Jiang, M. J.; Kim, M. J.; Xia, Y. N. Facile Synthesis of Bimetallic Nanoplates Consisting of Pd Cores and Pt Shells Through Seeded Epitaxial Growth. *Nano Lett.* **2008**, *8*, 2535−2540.
(22) Jiang, M. J.; Lim, B.; Tao, J.; Camargo, P. H. C.; Ma, C.; Zhu, Y. M.; Xia, Y. N. Epitaxial Overgrowth of Platinum on Palladium Nanocrystals. *Nanoscale* **2010**, *2*, 2406−2411.
(23) Zhang, H.; Jin, M. S.; Wang, J. G.; Kim, M. J.; Yang, D. R.; Xia, Y. N. Nanocrystals Composed of Alternating Shells of Pd and Pt Can Be Obtained by Sequentially Adding Different Precursors. *J. Am. Chem. Soc.* **2011**, *133*, 10422−10425.
(24) Tsuji, M.; Ikedo, K.; Matsunaga, M.; Uto, K. Epitaxial Growth of Au@Pd Core−Shell Nanocrystals Prepared Using a PVP-Assisted Polyol Reduction Method. *CrystEngComm* **2012**, *14*, 3411−3423.
(25) Lu, C. L.; Prasad, K. S.; Wu, H. L.; Ho, J. A. A.; Huang, M. H. Au Nanocube-Directed Fabrication of Au−Pd Core−Shell Nanocrystals with Tetrahexahedral, Concave Octahedral, and Octahedral Structures and Their Electrocatalytic Activity. *J. Am. Chem. Soc.* **2010**, *132*, 14546−14553.
(26) Lee, Y. W.; Kim, M.; Kim, Z. H.; Han, S. W. One-Step Synthesis of Au@Pd Core−Shell Nanooctahedron. *J. Am. Chem. Soc.* **2009**, *131*, 17036−17037.
(27) Wang, F.; Sun, L. D.; Feng, W.; Chen, H. J.; Yeung, M. H.; Wang, J. F.; Yan, C. H. Heteroepitaxial Growth of Core−Shell and Core-Multishell Nanocrystals Composed of Palladium and Gold. *Small* **2010**, *6*, 2566−2575.
(28) Xiang, Y. J.; Wu, X. C.; Liu, D. F.; Jiang, X. Y.; Chu, W. G.; Li, Z. Y.; Ma, Y.; Zhou, W. Y.; Xie, S. S. Formation of Rectangularly Shaped Pd/Au Bimetallic Nanorods: Evidence for Competing Growth of the Pd Shell Between the {110} and {100} Side Facets of Au Nanorods. *Nano Lett.* **2006**, *6*, 2290−2294.
(29) Kim, D. Y.; Choi, K. W.; Zhong, X. L.; Li, Z. Y.; Im, S. H.; Park, O. O. Au@Pd Core−Shell Nanocubes with Finely-Controlled Sizes. *CrystEngComm* **2013**, *15*, 3385−3391.
(30) DeSantis, C. J.; Weiner, R. G.; Radmilovic, A.; Bower, M. M.; Skrabalak, S. E. Seeding Bimetallic Nanostructures as a New Class of Plasmonic Colloids. *J. Phys. Chem. Lett.* **2013**, *4*, 3072−3082.
(31) Jin, M. S.; Zhang, H.; Wang, J. G.; Zhong, X. L.; Lu, N.; Li, Z. Y.; Xie, Z. X.; Kim, M. J.; Xia, Y. N. Copper Can Still Be Epitaxially Deposited on Palladium Nanocrystals To Generate Core−Shell Nanocubes Despite Their Large Lattice Mismatch. *ACS Nano* **2012**, *6*, 2566−2573.
(32) Tsuji, M.; Ikedo, K.; Uto, K.; Matsunaga, M.; Yoshida, Y.; Takemura, K.; Niidome, Y. Formation of Au@Pd@Cu Core−Shell Nanorods from Au@Pd Nanorods Through a New Stepwise Growth Mode. *CrystEngComm* **2013**, *15*, 6553−6563.
(33) Tsuji, M.; Yamaguchi, D.; Matsunaga, M.; Alam, M. J. Epitaxial Growth of Au@Cu Core−Shell Nanocrystals Prepared Using the PVP-Assisted Polyol Reduction Method. *Cryst. Growth Des.* **2010**, *10*, 5129−5135.
(34) Tsuji, M.; Yamaguchi, D.; Matsunaga, M.; Ikedo, K. Epitaxial Growth of Au@Ni Core−Shell Nanocrystals Prepared Using a Two-Step Reduction Method. *Cryst. Growth Des.* **2011**, *11*, 1995−2005.
(35) Zhang, J. T.; Tang, Y.; Lee, K.; Ouyang, M. Nonepitaxial Growth of Hybrid Core−Shell Nanostructures with Large Lattice Mismatches. *Science* **2010**, *327*, 1634−1638.
(36) Sun, Z. H.; Yang, Z.; Zhou, J. H.; Yeung, M. H.; Ni, W. H.; Wu, H. K.; Wang, J. F. A General Approach to the Synthesis of Gold-Metal Sulfide Core−Shell and Heterostructures. *Angew. Chem., Int. Ed.* **2009**, *48*, 2881−2885.
(37) Sun, H.; He, J. T.; Wang, J. Y.; Zhang, S. Y.; Liu, C. C.; Sritharan, T.; Mhaisalkar, S.; Han, M. Y.; Wang, D.; Chen, H. Y. Investigating the Multiple Roles of Polyvinylpyrrolidone for a General Methodology of Oxide Encapsulation. *J. Am. Chem. Soc.* **2013**, *135*, 9099−9110.
(38) Zhang, L.; Blom, D. A.; Wang, H. Au−Cu_2O Core−Shell Nanoparticles: A Hybrid Metal-Semiconductor Heteronanostructure with Geometrically Tunable Optical Properties. *Chem. Mater.* **2011**, *23*, 4587−4598.
(39) Chen, W. T.; Yang, T. T.; Hsu, Y. J. Au−CdS Core−Shell Nanocrystals with Controllable Shell Thickness and Photoinduced Charge Separation Property. *Chem. Mater.* **2008**, *20*, 7204−7206.
(40) Tian, Z. Q.; Zhang, Z. L.; Jiang, P.; Zhang, M. X.; Xie, H. Y.; Pang, D. W. Core/Shell Structured Noble Metal (Alloy)/Cadmium Selenide Nanocrystals. *Chem. Mater.* **2009**, *21*, 3039−3041.
(41) Li, M.; Yu, X. F.; Liang, S.; Peng, X. N.; Yang, Z. J.; Wang, Y. L.; Wang, Q. Q. Synthesis of Au−CdS Core−Shell Hetero-Nanorods with Efficient Exciton-Plasmon Interactions. *Adv. Funct. Mater.* **2011**, *21*, 1788−1794.
(42) Lee, J. S.; Shevchenko, E. V.; Talapin, D. V. Au−PbS Core−Shell Nanocrystals: Plasmonic Absorption Enhancement and Electrical Doping via Intra-Particle Charge Transfer. *J. Am. Chem. Soc.* **2008**, *130*, 9673−9675.
(43) Park, G.; Lee, C.; Seo, D.; Song, H. Full-Color Tuning of Surface Plasmon Resonance by Compositional Variation of Au@Ag Core−Shell Nanocubes with Sulfides. *Langmuir* **2012**, *28*, 9003−9009.
(44) Vasa, P.; Pomraenke, R.; Schwieger, S.; Mazur, Y. I.; Kunets, V.; Srinivasan, P.; Johnson, E.; Kihm, J. E.; Kim, D. S.; Runge, E.; et al. Coherent Exciton-Surface-Plasmon-Polariton Interaction in Hybrid Metal-Semiconductor Nanostructures. *Phys. Rev. Lett.* **2008**, *101*, 116801.
(45) Chen, H. J.; Shao, L.; Man, Y. C.; Zhao, C. M.; Wang, J. F.; Yang, B. C. Fano Resonance in (Gold Core)-(Dielectric Shell) Nanostructures Without Symmetry Breaking. *Small* **2012**, *8*, 1503−1509.
(46) Kuo, C. H.; Yang, Y. C.; Gwo, S.; Huang, M. H. Facet-Dependent and Au Nanocrystal-Enhanced Electrical and Photocatalytic Properties of Au−Cu_2O Core−Shell Heterostructures. *J. Am. Chem. Soc.* **2011**, *133*, 1052−1057.
(47) Wang, W. C.; Lyu, L. M.; Huang, M. H. Investigation of the Effects of Polyhedral Gold Nanocrystal Morphology and Facets on the Formation of Au−Cu_2O Core−Shell Heterostructures. *Chem. Mater.* **2011**, *23*, 2677−2684.
(48) Yang, Y. C.; Wang, H. J.; Whang, J.; Huang, J. S.; Lyu, L. M.; Lin, P. H.; Gwo, S.; Huang, M. H. Facet-Sependent Optical Properties of Polyhedral Au−Cu_2O Core−Shell Nanocrystals. *Nanoscale* **2014**, *6*, 4316−4324.
(49) Kuo, C. H.; Hua, T. E.; Huang, M. H. Au Nanocrystal-Directed Growth of Au−Cu_2O Core−Shell Heterostructures with Precise Morphological Control. *J. Am. Chem. Soc.* **2009**, *131*, 17871−17878.
(50) Zhang, L.; Jing, H.; Boisvert, G.; He, J. Z.; Wang, H. Geometry Control and Optical Tunability of Metal-Cuprous Oxide Core−Shell Nanoparticles. *ACS Nano* **2012**, *6*, 3514−3527.
(51) Liu, D. Y.; Ding, S. Y.; Lin, H. X.; Liu, B. J.; Ye, Z. Z.; Fan, F. R.; Ren, B.; Tian, Z. Q. Distinctive Enhanced and Tunable Plasmon Resonant Absorption from Controllable Au@Cu_2O Nanoparticles: Experimental and Theoretical Modeling. *J. Phys. Chem. C* **2012**, *116*, 4477−4483.
(52) Cushing, S. K.; Li, J. T.; Meng, F. K.; Senty, T. R.; Suri, S.; Zhi, M. J.; Li, M.; Bristow, A. D.; Wu, N. Q. Photocatalytic Activity Enhanced by Plasmonic Resonant Energy Transfer from Metal to Semiconductor. *J. Am. Chem. Soc.* **2012**, *134*, 15033−15041.
(53) Li, J. T.; Cushing, S. K.; Bright, J.; Meng, F. K.; Senty, T. R.; Zheng, P.; Bristow, A. D.; Wu, N. Q. Ag@Cu_2O Core−Shell Nanoparticles as Visible-Light Plasmonic Photocatalysts. *ACS Catal.* **2013**, *3*, 47−51.
(54) Meir, N.; Plante, I. J. L.; Flomin, K.; Chockler, E.; Moshofsky, B.; Diab, M.; Volokh, M.; Mokari, T. Studying the Chemical, Optical and Catalytic Properties of Noble Metal (Pt, Pd, Ag, Au)-Cu_2O Core−Shell Nanostructures Grown via a General Approach. *J. Mater. Chem. A* **2013**, *1*, 1763−1769.
(55) Kong, L. N.; Chen, W.; Ma, D. K.; Yang, Y.; Liu, S. S.; Huang, S. M. Size Control of Au@Cu_2O Octahedra for Excellent Photocatalytic Performance. *J. Mater. Chem.* **2012**, *22*, 719−724.

(56) Wang, Y. Q.; Nikitin, K.; McComb, D. W. Fabrication of Au–Cu_2O Core–Shell Nanocube Heterostructures. *Chem. Phys. Lett.* **2008**, *456*, 202–205.
(57) Johnson, P. B.; Christy, R. W. Optical Constants of Noble Metals. *Phys. Rev. B* **1972**, *6*, 4370–4379.
(58) Kumbhar, A. S.; Kinnan, M. K.; Chumanov, G. Multipole Plasmon Resonances of Submicron Silver Particles. *J. Am. Chem. Soc.* **2005**, *127*, 12444–12445.
(59) Sherry, L. J.; Chang, S. H.; Schatz, G. C.; Van Duyne, R. P.; Wiley, B. J.; Xia, Y. N. Localized Surface Plasmon Resonance Spectroscopy of Single Silver Nanocubes. *Nano Lett.* **2005**, *5*, 2034–2038.
(60) Ringe, E.; McMahon, J. M.; Sohn, K.; Cobley, C.; Xia, Y. N.; Huang, J. X.; Schatz, G. C.; Marks, L. D.; Van Duyne, R. P. Unraveling the Effects of Size, Composition, and Substrate on the Localized Surface Plasmon Resonance Frequencies of Gold and Silver Nanocubes: A Systematic Single-Particle Approach. *J. Phys. Chem. C* **2010**, *114*, 12511–12516.
(61) Zhou, F.; Li, Z. Y.; Liu, Y.; Xia, Y. N. Quantitative Analysis of Dipole and Quadrupole Excitation in the Surface Plasmon Resonance of Metal Nanoparticles. *J. Phys. Chem. C* **2008**, *112*, 20233–20240.
(62) Tao, A.; Sinsermsuksakul, P.; Yang, P. D. Polyhedral Silver Nanocrystals with Distinct Scattering Signatures. *Angew. Chem., Int. Ed.* **2006**, *45*, 4597–4601.
(63) Wei, H.; Reyes-Coronado, A.; Nordlander, P.; Aizpurua, J.; Xu, H. X. Multipolar Plasmon Resonances in Individual Ag Nanorice. *ACS Nano* **2010**, *4*, 2649–2654.
(64) Chen, B.; Jiao, X. L.; Chen, D. R. Size-Controlled and Size-Designed Synthesis of Nano/Submicrometer Ag Particles. *Cryst. Growth Des.* **2010**, *10*, 3378–3386.
(65) Xia, X. H.; Zeng, J.; Oetjen, L. K.; Li, Q. G.; Xia, Y. N. Quantitative Analysis of the Role Played by Poly(vinylpyrrolidone) in Seed-Mediated Growth of Ag Nanocrystals. *J. Am. Chem. Soc.* **2012**, *134*, 1793–1801.
(66) Ye, X. C.; Jin, L. H.; Caglayan, H.; Chen, J.; Xing, G. Z.; Zheng, C.; Vicky, D. N.; Kang, Y. J.; Engheta, N.; Kagan, C. R.; et al. Improved Size-Tunable Synthesis of Monodisperse Gold Nanorods Through the Use of Aromatic Additives. *ACS Nano* **2012**, *6*, 2804–2817.
(67) Jiang, R. B.; Chen, H. J.; Shao, L.; Li, Q.; Wang, J. F. Unraveling the Evolution and Nature of the Plasmons in (Au core)–(Ag shell) Nanorods. *Adv. Mater.* **2012**, *24*, OP200–OP207.
(68) Palik, E. D. *Handbook of Optical Constants of Solids*; Academic Press: San Diego, CA, 1985; Vol. *1*.
(69) Collaboration: Authors and editors of the volumes III/17E-17F-41C: Cuprous oxide (Cu_2O) dielectric constant. Madelung, O., Rössler, U., Schulz, M., Eds.; SpringerMaterials—The Landolt–Börnstein Database (http://www.springermaterials.com). DOI: 10.1007/10681727_58.
(70) Li, H. S.; Xia, H. B.; Ding, W. C.; Li, Y. J.; Shi, Q. R.; Wang, D. Y.; Tao, X. T. Synthesis of Monodisperse, Quasi-Spherical Silver Nanoparticles with Sizes Defined by the Nature of Silver Precursors. *Langmuir* **2014**, *30*, 2498–2504.
(71) Bastús, N. G.; Merkoçi, F.; Piella, J.; Puntes, V. Synthesis of Highly Monodisperse Citrate-Stabilized Silver Nanoparticles of Up to 200 nm: Kinetic Control and Catalytic Properties. *Chem. Mater.* **2014**, *26*, 2836–2846.
(72) Williams, D. B.; Carter, C. B. *Transmission Electron Microscopy, a Text for Materials Science*; Plenum Press: New York, 1996.
(73) Grzelczak, M.; Rodriguez-Gonzalez, B.; Perez-Juste, J.; Liz-Marzan, L. M. Quasi-Epitaxial Growth of Ni Nanoshells on Au Nanorods. *Adv. Mater.* **2007**, *19*, 2262–2266.
(74) Zhang, L.; Wang, H. Interior Structural Tailoring of Cu_2O Shell-in-Shell Nanostructures Through Multistep Ostwald Ripening. *J. Phys. Chem. C* **2011**, *115*, 18479–18485.
(75) Zhang, L.; Wang, H. Cuprous Oxide Nanoshells with Geometrically Tunable Optical Properties. *ACS Nano* **2011**, *5*, 3257–3267.
(76) Qiu, C.; Zhang, L.; Wang, H.; Jiang, C. Y. Surface-Enhanced Raman Scattering on Hierarchical Porous Cuprous Oxide Nanostructures in Nanoshell and Thin-Film Geometries. *J. Phys. Chem. Lett.* **2012**, *3*, 651–657.
(77) Westcott, S. L.; Jackson, J. B.; Radloff, C.; Halas, N. J. Relative Contributions to the Plasmon Line Shape of Metal Nanoshells. *Phys. Rev. B* **2002**, *66*, 155431.
(78) Wang, H.; Halas, N. J. Mesoscopic Au "Meatball" Particles. *Adv. Mater.* **2008**, *20*, 820–825.
(79) Rodriguez-Fernandez, J.; Perez-Juste, J.; de Abajo, F. J. G.; Liz-Marzan, L. M. Seeded Growth of Submicron Au Colloids with Quadrupole Plasmon Resonance Modes. *Langmuir* **2006**, *22*, 7007–7010.
(80) Zhou, F.; Liu, Y.; Li, Z. Y. Simultaneous Low Extinction and High Local Field Enhancement in Ag Nanocubes. *Chin. Phys. B* **2011**, *20*, 037303.
(81) Hermoso, W.; Alves, T. V.; Ornellas, F. R.; Camargo, P. H. C. Comparative Study on the Far-Field Spectra and Near-Field Amplitudes for Silver and Gold Nanocubes Irradiated at 514, 633 and 785 nm as a Function of the Edge Length. *Eur. Phys. J. D* **2012**, *66*, 135.
(82) Liu, Y.; Huang, C. Z. Screening Sensitive Nanosensors via the Investigation of Shape-Dependent Localized Surface Plasmon Resonance of Single Ag Nanoparticles. *Nanoscale* **2013**, *5*, 7458–7466.
(83) Mahmoud, M. A.; Chamanzar, M.; Adibi, A.; El-Sayed, M. A. Effect of the Dielectric Constant of the Surrounding Medium and the Substrate on the Surface Plasmon Resonance Spectrum and Sensitivity Factors of Highly Symmetric Systems: Silver Nanocubes. *J. Am. Chem. Soc.* **2012**, *134*, 6434–6442.
(84) Kuo, C. H.; Huang, M. H. Morphologically Controlled Synthesis of Cu_2O Nanocrystals and Their Properties. *Nano Today* **2010**, *5*, 106–116.
(85) Li, B.; Long, R.; Zhong, X. L.; Bai, Y.; Zhu, Z. J.; Zhang, X.; Zhi, M.; He, J. W.; Wang, C. M.; Li, Z. Y.; et al. Investigation of Size-Dependent Plasmonic and Catalytic Properties of Metallic Nanocrystals Enabled by Size Control with HCl Oxidative Etching. *Small* **2012**, *8*, 1710–1716.
(86) Okuno, Y.; Nishioka, K.; Kiya, A.; Nakashima, N.; Ishibashi, A.; Niidome, Y. Uniform and Controllable Preparation of Au–Ag Core–Shell Nanorods Using Anisotropic Silver Shell Formation on Gold Nanorods. *Nanoscale* **2010**, *2*, 1489–1493.
(87) Cortie, M. B.; Liu, F. G.; Arnold, M. D.; Niidome, Y. Multimode Resonances in Silver Nanocuboids. *Langmuir* **2012**, *28*, 9103–9112.